

3 Ion Trap Implementations

Single atoms or ions in vacuum chambers represent a very well isolated and controllable quantum system. Lasers offer an almost ideal tool to manipulate and also to detect qubits which are encoded in atomic states. We will concentrate here on experiments with trapped ions. Other proposals suggest the use of neutral atoms and optical lattices.

3.1 Trapping Ions

3.1.1 Paul traps

It is well known from the so-called Earnshaw theorem that a charged particle cannot be trapped in a stable configuration with static electric fields only. However, a combination of static electric and magnetic fields (**Penning trap**) or time dependent electric fields (**Paul trap**) can provide space points where a restoring force in all three directions acts on a charged particle.

A Paul trap (Nobel Prize 1989) consists of two parabolical electrodes and a ring electrode.

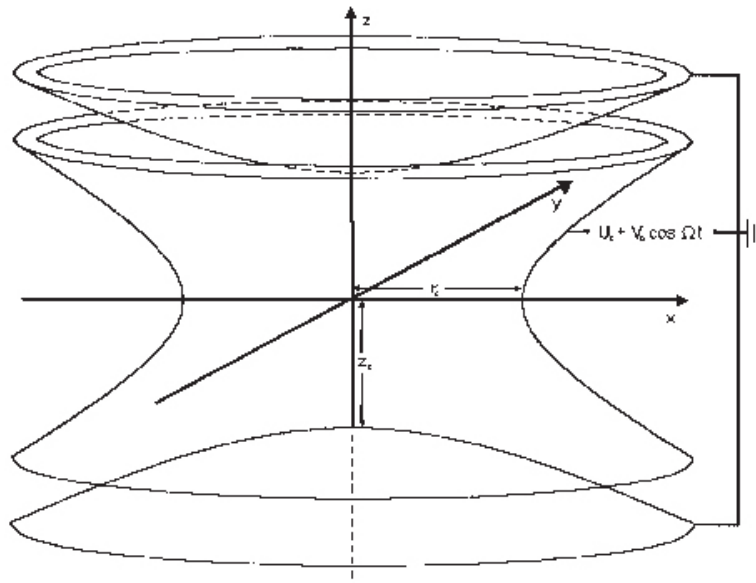


Figure 28: Sketch of a Paul trap

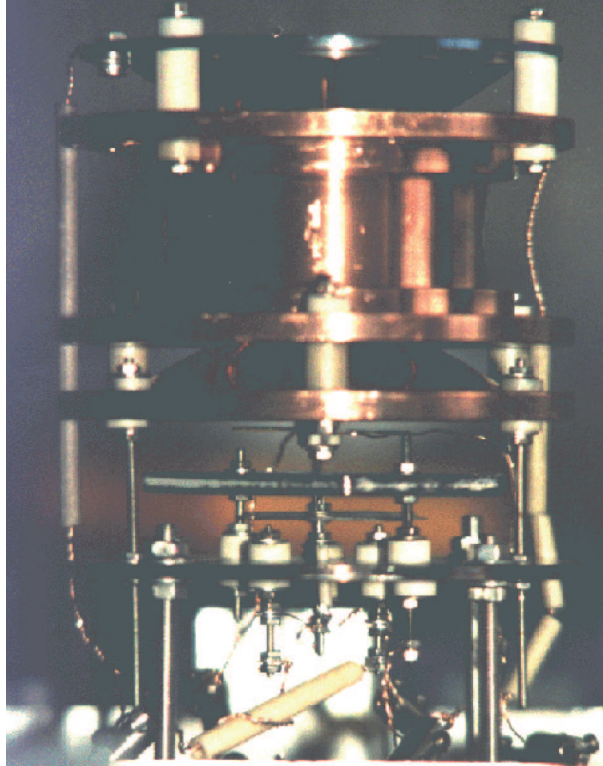


Figure 29: Photo of a Paul trap [from <http://www.physik.uni-mainz.de>]

If a dc-voltage U_{dc} and an ac-voltage V_{ac} of frequency Ω is applied to the electrodes then the potential near the trap axis is of the form:

$$\Phi = \frac{(U_{dc} + V_{ac} \cos(\Omega t))(r^2 - 2z^2 + 2z_0^2)}{r_0^2 + 2z_0^2}$$

where r_0 and z_0 denote the distances from the trap axis to the surface of the electrodes.

The potential is harmonic and for a certain time t provides a restoring force in one dimension.

Say, at a given time t the x-direction is the non-confining direction. Then, due to its inertia a particle cannot escape along that direction before the sign of $\cos(\Omega t)$ is inverted, and the x-direction becomes the confining direction. For

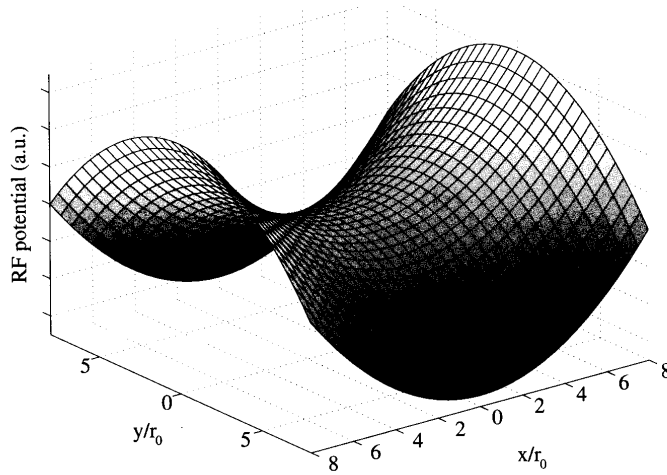


Figure 30: Paul trap potential [from Bouwmeester et al.]

certain frequencies Ω this results in an effective confinement in all three directions.

The equations of motion in a Paul trap are:

$$m \frac{d^2}{dt^2} \begin{pmatrix} x \\ y \\ z \end{pmatrix} = \frac{2q(U_{dc} - V_{ac} \cos(\omega t))}{r_0^2 + 2z_0^2} \begin{pmatrix} -x \\ -y \\ 2z \end{pmatrix}$$

With the transformation

$$\begin{aligned} \tau &= 1/2\omega \\ a_x &= a_y = -a_z/2 = \frac{4qU_{dc}}{mr_0^2\Omega^2} \\ q_x &= q_y = -q_z/2 = \frac{2qV_{ac}}{m\Omega^2r_0^2} \end{aligned}$$

one finds the *Mathieu equations*:

$$\frac{d^2 u_i}{d\tau^2} + (a_i + 2q_i \cos(2\tau)) u_i = 0$$

with $i = x, y, z$

For the approximation $a_i < q_i \ll 1$, which is usually fulfilled, there exists an

analytic solution:

$$u_i(t) = A_i \cos(\Omega_i t + \phi_i) \left[1 + \frac{q_i}{2} \cos(\omega t) \right]$$

The solution consist of a rapid oscillation with the trap frequency ω , the so-called *micromotion*, and a slower *macromotion* (or *secular motion*) at frequency Ω_i in the effective harmonic trap potential with:

$$\Omega_i \approx \frac{\omega}{2} \left(a_i + \frac{q_i}{2} \right)$$

In the trap center the micromotion vanishes completely.

As an example of a very fundamental experiment with single trapped ions Fig. 32 shows the fluorescence from a single Ba-Ion.

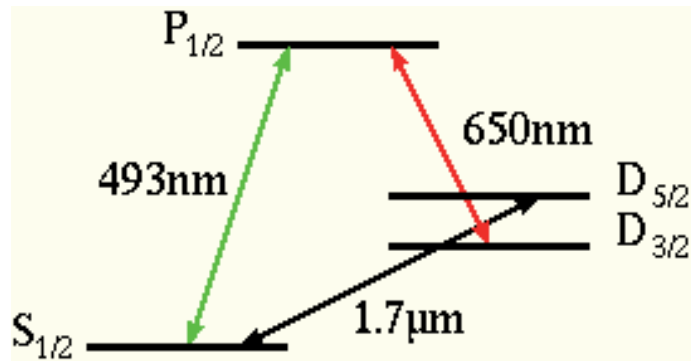


Figure 31: Energy levels of Ba

If a single ion is trapped and continuously illuminated with laser light (here on the $P_{1/2} \rightarrow S_{1/2}$ transition, see Fig. refBalevels) then the fluorescence vanishes abruptly due to transitions to the metastable $D_{5/2}$ level (The other arrow indicates repumping from the $D_{3/2}$ level). First experiments were performed in 1986. The possibility to observe these "Quantum Jumps" led to many theoretical discussions in the early 50's.

3.1.2 Trapping ion strings

In order to realize quantum computers it is required to store many ions. *Linear ion traps* are modifications of the single-ion Paul trap. These traps usually consist of two pairs of electrodes (hyperbolically shaped, spherical rods, or rectangular shapes) which provide a confinement in two directions. These configurations resemble mass spectrometers (more precisely e/m filters). A second

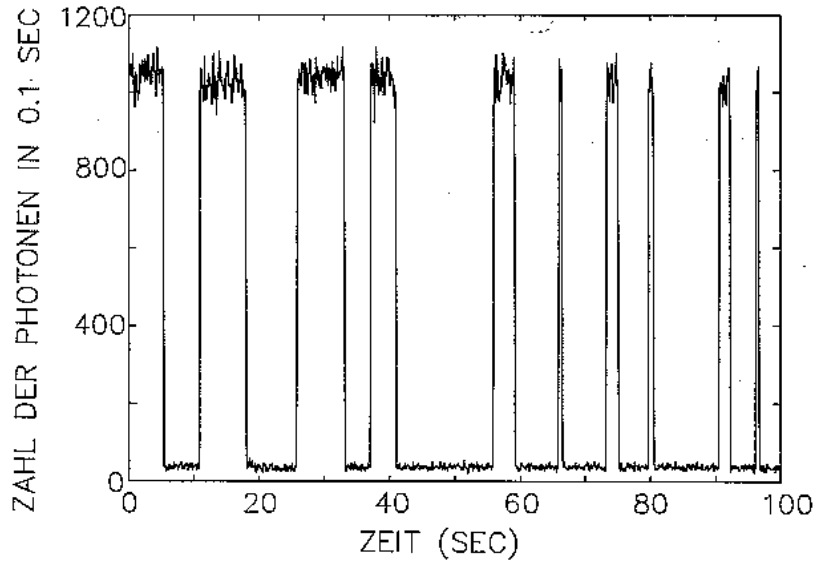


Figure 32: Quantum jumps of a single Ba-atom[from <http://www.physnet.uni-hamburg.de/ilp/toschek/ionen.html>]

pair of end cap electrodes provides the confinement in the orthogonal direction. Figure 33 shows various configurations.

In a linear trap the equation of motion in z -direction (direction of the end caps) is given by:

$$\frac{d^2 u_z}{dt^2} + (2\kappa q U_{cap} / m z_0^2) u_z = 0$$

where q, m are the charge and mass of the ion and κ is an empirically found parameter.

The equation of motion in the orthogonal directions is given again by the Mathieu equations:

$$\frac{d^2 u_i}{d\tau^2} + (a_i + 2q_i \cos(2\tau)) u_i = 0$$

with $i = x, y$

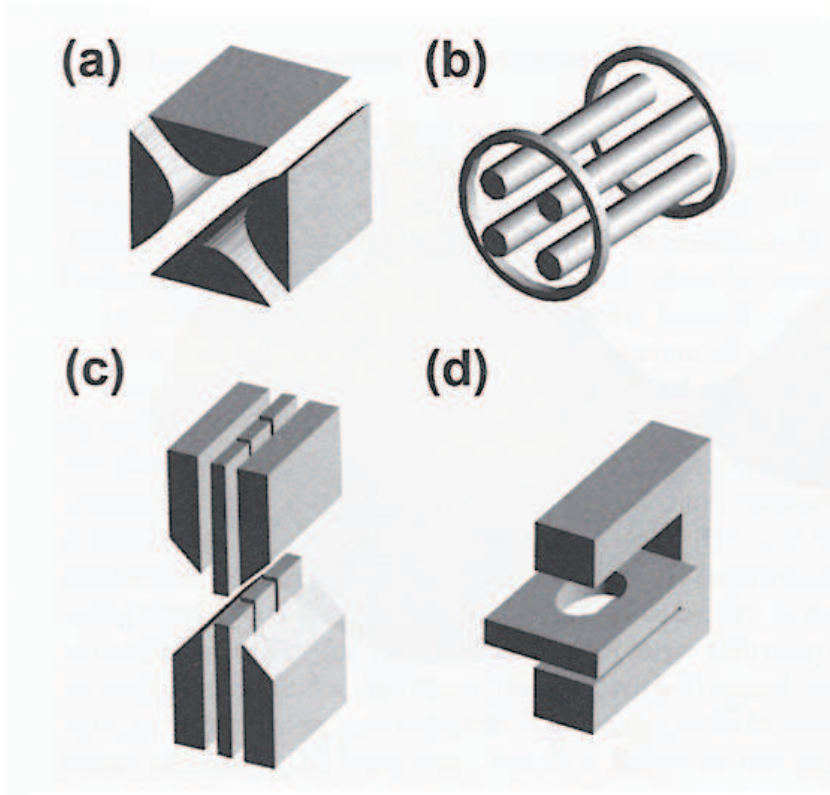


Figure 33: Different types of linear ion traps [from Bouwmeester et al.]

where

$$\begin{aligned}
 a_x &= \frac{4q}{m\Omega^2} \left(\frac{U_{dc}}{r_0^2} - \frac{\kappa U_{cap}}{z_0^2} \right) \\
 a_y &= -\frac{4q}{m\Omega^2} \left(\frac{U_{dc}}{r_0^2} + \frac{\kappa U_{cap}}{z_0^2} \right) \\
 q_x &= -q_y = \frac{2qV_{ac}}{m\Omega^2 r_0^2} \\
 \tau &= \Omega t / 2
 \end{aligned}$$

Similar as in the single-ion trap the motion of the ions can be approximated as a combination of micro- and macromotion. What is important now is that *the micromotion vanishes completely on the whole trap axis!*

Figure34 The following shows a collection of pictures (raw video data) of stored

Ca-ion strings. The images were taken with CCD cameras:

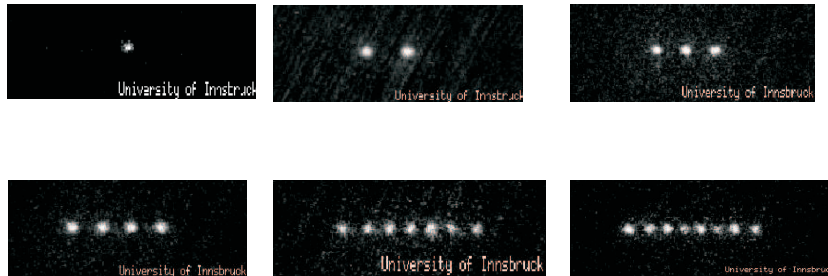


Figure 34: Strings of ions stored in a linear Paul trap [from <http://heart-c704.uibk.ac.at/>]

3.1.3 Normal Modes

If the radial confinement in a linear ion trap is strong enough, ions arrange in a linear pattern along the trap axis at low temperatures. The distance between the ions is determined by the equilibrium of the Coulomb repulsion and the potential providing axial confinement.

Small displacements of the ions from their equilibrium position cannot be described in terms of the motion of individual ions since the Coulomb interaction couples the charged particles. Instead, the motion of the string must be described in terms of *normal modes*.

- One example of a normal mode is the *center-of-mass* (COM) mode of the string. This corresponds to an oscillation of the whole string as if all ions were rigidly joined.
- Another example is the *breathing mode*. It describes an oscillation where the ions move in opposite directions and leave the COM fixed.
- The spectrum of other higher order modes can be calculated from the trap parameters.

The following figure shows the experimental observation of the COM mode and the breathing mode of a string of 7 Ca atoms which were excited via the trap's end cap electrodes:

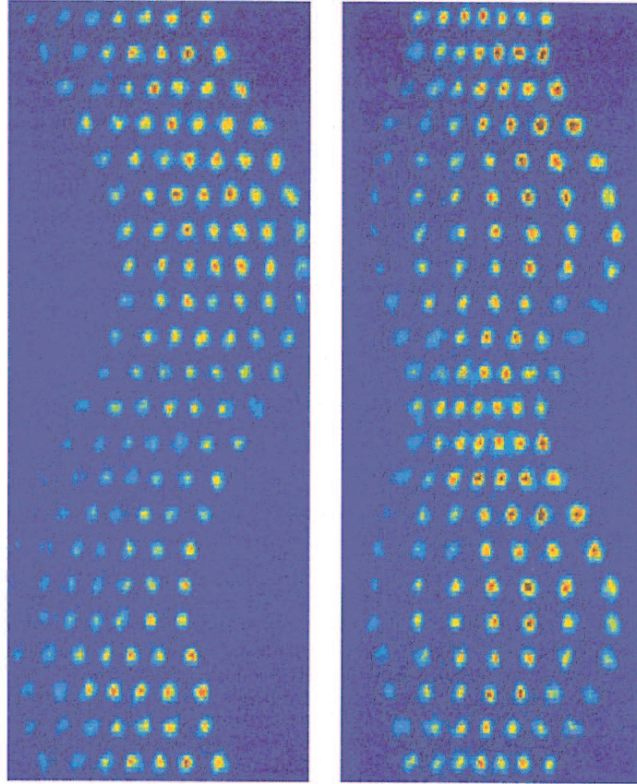


Figure 35: Excitation of normal modes in a string of 7 Ca atoms [from Bouwmeester et al.]

3.2 Laser Cooling

If a string of trapped ions should be used for quantum computaion it is required to cool ions down to the ground state of their normal modes. (More recent proposal have weakened this requirement, but cooling is yet desirable).

With laser cooling (Nobel prize for Chu, Cohen-Tannoudji, Phillips) temperatures which are far beyond reach of cryostats could be realized.

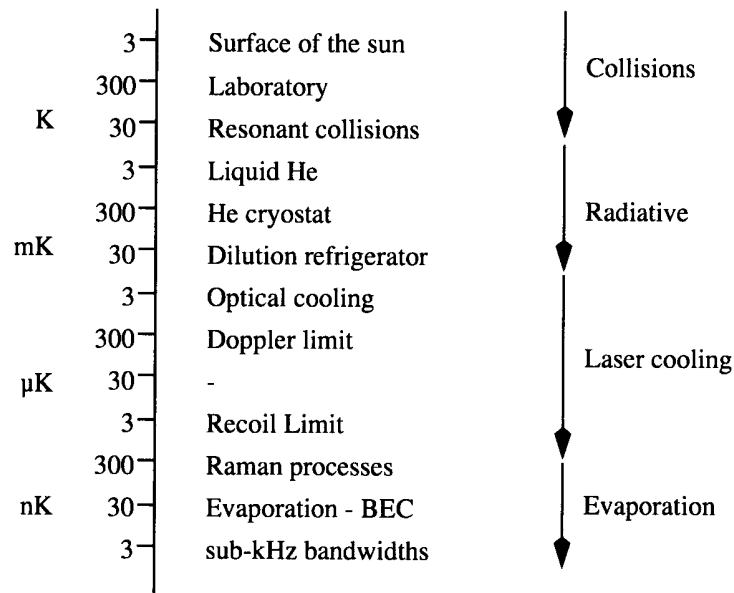


Figure 36: Temperature scale [from H. J. Metcalf, P. van der Straten, "Laser Cooling and Trapping", Springer N.Y. 2002]

The definition of "temperature" in laser cooling requires some discussion. It is used to describe an atomic sample whose average kinetic energy $\langle E_k \rangle$ has been reduced by laser cooling. The label "temperature" now is written as:

$$\frac{1}{2}k_B T = \langle E_k \rangle$$

with Boltzmann's constant k_B .

3.2.1 Doppler Cooling

The idea of laser cooling is illustrated by the following figure:

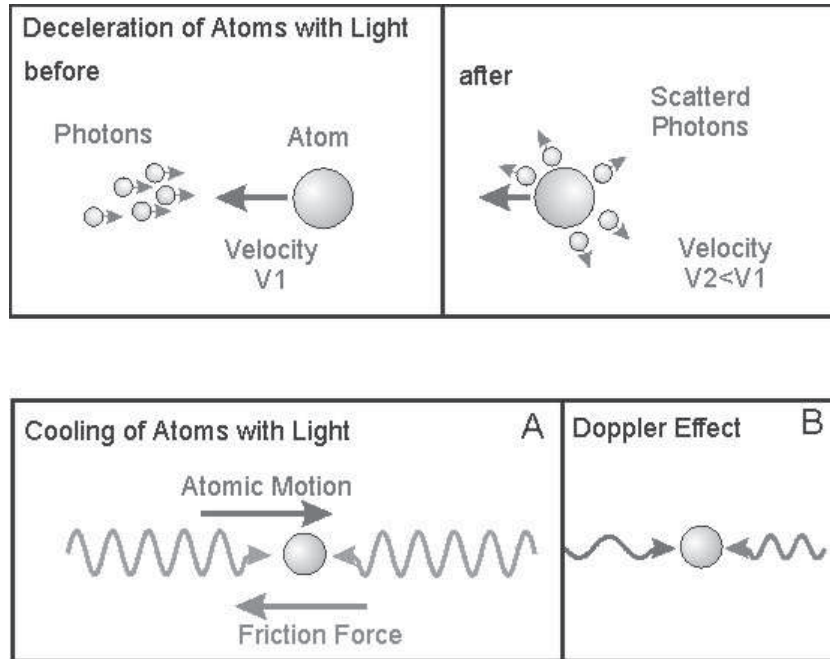


Figure 37: Schematics of laser cooling

Assume a moving atom is interacting with monochromatic laser which is red detuned from the resonance of an electronic transition of the atom. Then, the atom can only absorb photons from the laser light if it moves towards the laser and is thus tuned to resonance by the Doppler shift. The atom experiences a momentum change Δp which causes a deceleration. After absorption the atom spontaneously emits the photon again. Since spontaneous emission is isotropic there is no momentum change *on the average*. Two laser beams from opposite directions can thus decelerate or cool the atomic motion in one direction. Accordingly, three pairs of laser beams establish a cooling in all three directions. The minimum temperature achievable in this way by *Doppler cooling* is the *Doppler temperature*:

$$k_B T_D = \frac{\hbar \Gamma}{2}$$

where Γ is the natural linewidth of the transition.

The achievable deceleration is remarkable: An atom moving with a thermal velocity of 1000 m/sec can be stopped within a ms. This correspond roughly to 10^5 g!

3.2.2 Harmonic potential

As pointed out above the trap potential for ions in a Paul trap is usually harmonic close to the trap's center. The Hamiltonian of a particle in a one dimensional harmonic potential is:

$$H = \frac{p^2}{2m} + \frac{1}{2}m\omega^2 x^2$$

with the definition of the creation and annihilation operator a^\dagger, a

$$\begin{aligned} a &= \frac{1}{\sqrt{2m\hbar\omega}} (m\omega x + ip) \\ a^\dagger &= \frac{1}{\sqrt{2m\hbar\omega}} (m\omega x - ip) \end{aligned}$$

with the properties

$$\begin{aligned} a^\dagger |n\rangle &= \sqrt{n+1} |n+1\rangle \\ a |n\rangle &= \sqrt{n} |n-1\rangle \end{aligned}$$

one derives the Hamiltonian of the harmonic oscillator:

$$H = \hbar\omega \left(a^\dagger a + \frac{1}{2} \right)$$

The motional eigenstates of a trapped particle are thus harmonic oscillator eigenstates with equally spaced eigenvalues and sometimes similar as quantized lattice vibrations called *phonons*. The typical length scale x_0 is:

$$x_0 = \sqrt{\hbar/2m\omega}$$

3.2.3 Sideband Cooling

In a trap potential ions can be cooled down even further than the Doppler limit by the so-called **sideband cooling**. Figure 38 illustrates how this works:

The lowest picture shows the typical energy structure of an ion in a trap. It is a combination of the ion's two internal states (e and g) and the motional states. A laser is tuned to a transition to an excited state with a lower motional excitation. Spontaneous emission now causes a transition without change of the

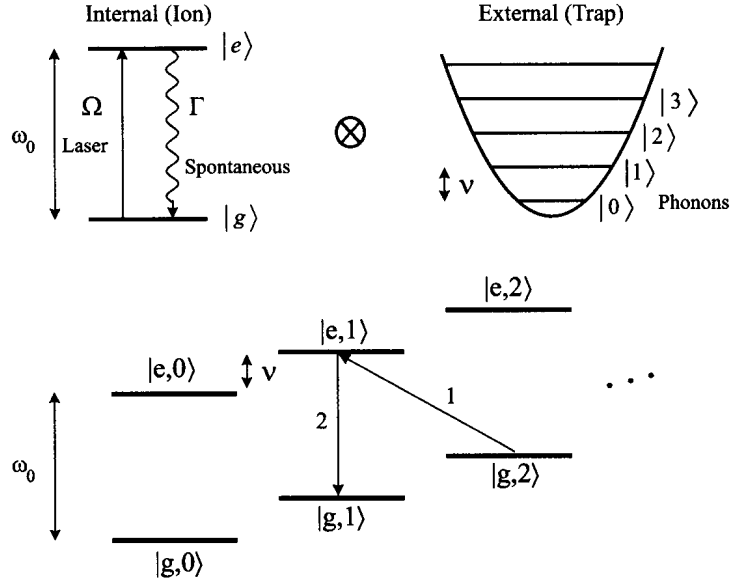


Figure 38: Schematics of sideband-cooling [from Bouwmeester et al.]

motional state (on the average). Since the potential is harmonic this scheme applies to all pairs of neighboring motional states. Motional quanta are removed one-by-one in each optical cycle, and the ion ends up in the motional ground state which is then decoupled from the laser light.

In experimental realizations either a stabilized laser is used to resolve individual sidebands or a Raman transition where the energy difference between two incident lasers equals the energy of one phonon.

3.2.4 Choosing atoms

Although an ion trap is very deep (several eV potential well depth) and will hold almost every ion, only a few ions are suitable for quantum computation. The following requirements should be met:

- The electronic level structure should be simple to allow the realization of a closed two level system without the need of too many lasers.
- The levels used for the qubit transition should have a negligible decoherence (e.g. by spontaneous decay).
- The levels should allow for efficient laser cooling and detection (some strong transitions).

Because of these requirements the ions of choice have typically only one electron in the outer shell (hydrogenic ions). The two level system can either be provided by *two hyperfine ground states* or by a *ground state and a long-lived metastable electronic state*.

Most of the experiments have been done with ${}^9\text{Be}^+$ and ${}^{40}\text{Ca}^+$, but other possible ions are ${}^{138}\text{Ba}^+$, ${}^{25}\text{Mg}^+$, ${}^{199}\text{Hg}^+$, and ${}^{171}\text{Yb}^+$.

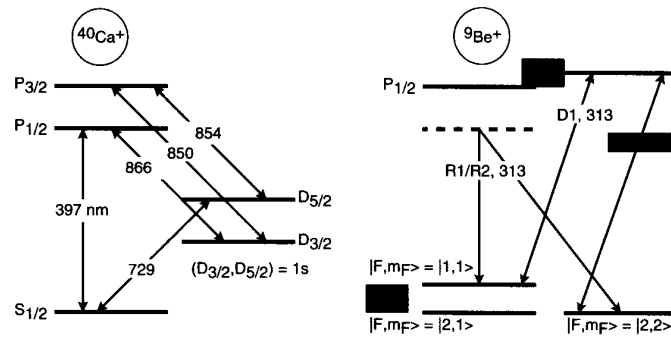


Figure 39: Energy levels of Ca and Be [from Bouwmeester et al.]

Cooling of the ions starts with Doppler cooling. In ${}^9\text{Be}^+$, the ultraviolet $S_{1/2} \rightarrow P_{3/2}$ transition at 313 nm is used, while for the ${}^{40}\text{Ca}^+$ the corresponding transition is 397 nm . Frequency doubled Ti:Sapphire or dye lasers are used to generate the UV light. (A major advantage of a specific ion could be whether it is possible to use cheap lasers, e.g. diode lasers for the optical excitations!)

The Doppler cooling leads to a thermal state of motion with a temperature of about 1 mK . Then, it depends on the trap depth how many motional states n_{phonon} are occupied at this temperature. The number ranges between $\langle n_{\text{phonon}} \rangle = 1.3$ ($\omega_{\text{trap}}/2\pi = 11\text{ MHz}$) and $\langle n_{\text{phonon}} \rangle = 50$ ($\omega_{\text{trap}}/2\pi = 140\text{ kHz}$). Subsequent sideband cooling cools the ions to the motional ground state.

3.3 Single and Two Qubit Gates

3.3.1 Hamiltonian of ions in a trap

The Hamiltonian of N ions in a 3-dimensional harmonic trap potential which interact via Coulomb interaction is:

$$H_{Nions} = \sum_{i=1}^N \frac{m}{2} \left(\omega_x x_i^2 + \omega_y y_i^2 + \omega_z z_i^2 + \frac{|p_i|^2}{2} \right) + \sum_{i=1}^N \sum_{i < j} \frac{e^2}{4\pi\epsilon_0(|\vec{r}_i - \vec{r}_j|)}$$

Since a typical trap potential in a linear ion trap is shallowest in the z -direction (i.e. perpendicular to the end caps) it is sufficient here to consider only the z -coordinate. The ions remain in the ground state with respect to the oscillation in both x - and y -direction.

The ions are laser cooled to the so-called *Lamb-Dicke regime*. The Lamb-Dicke regime is defined as $\eta \ll 1$, where η is the Lamb-Dicke parameter. This parameter gives the ratio between the typical length scale z_0 of an ion's oscillation amplitude in a harmonic trap potential and the wavelength λ of the incident laser radiation:

$$\eta = 2\pi z_0 / \lambda = 2\pi \sqrt{\hbar / 2Nm\omega_{trap}} / \lambda$$

where N is the number of ions in the trap, m the ion's mass, and ω_{trap} is the trap frequency.

If the ions are laser cooled they only perform small oscillations around their equilibrium position. Then the Coulomb potential can be expanded as a Taylor series. Thus, the potential (trap and Coulomb potential) along the z -direction can be written as:

$$V(z) = \sum_{i=1}^N \sum_{j=1}^N U_{ij} z_i z_j$$

The diagonalization of this potential can be achieved by transforming to the normal variables. Finally, the Hamiltonian H_{Nions} is transformed into

$$H_{Nions} = \sum_{i=1}^N \hbar\omega_i a_i^\dagger a_i$$

which is an harmonic oscillator potential for N *normal modes*.

3.3.2 Interaction with a laser field

The interaction of the ions in the trap with a classical laser field at frequency ω is now:

$$H_I^i = \Omega_i \cos(kz_i + \phi_i + \omega t) (\sigma_i^+ + \sigma_i^-)$$

Note here that we considered one particular normal mode i and assumed a standing wave laser field. The Rabi-frequency Ω_i is proportional to the amplitude of the classical laser field. σ_i^+ and σ_i^- describe the raising and lowering operators of the atom's two internal states.

The coordinate z_i is now quantized due to the motion in the trap potential:

$$z_i = z_{i,equilibrium} + 1/\sqrt{\hbar/2Nm\omega_{CM}}(a + a^\dagger)$$

Note: We consider only an excitation of the lowest (center-of-mass) normal mode. This introduces the factor of $1/\sqrt{N}$ to the normal coordinates. With the equilibrium position absorbed in the phase ϕ_i the Hamiltonian reads:

$$H_I^i = \Omega_i \cos\left(\frac{\eta}{\sqrt{N}}(a + a^\dagger) + \phi_i + \omega t\right)(\sigma_i^+ + \sigma_i^-)$$

In the limit of small Lamb-Dicke parameter, $\eta \ll 1$, one finds after some algebra two cases:

1. Laser tuned to the internal atomic transition $\omega = \omega_0$:

$$H_I^i = \Omega_i/2 (\sigma_i^+ \exp(i\phi_i) + \sigma_i^- \exp(-i\phi_i))$$

The laser field introduces only transitions between internal states of the ions.

2. Laser tuned to one of the sideband transitions $\omega = \omega_0 \pm \omega_{CM}$:

$$\begin{aligned} H_I^i &= \frac{\Omega_i}{2\sqrt{N}} (\sigma_i^+ a^\dagger \exp(i\phi_i) - \sigma_i^- a \exp(-i\phi_i)) \quad \text{if } \omega = \omega_0 + \omega_{CM} \\ H_I^i &= \frac{\Omega_i}{2\sqrt{N}} (\sigma_i^+ a \exp(i\phi_i) - \sigma_i^- a^\dagger \exp(-i\phi_i)) \quad \text{if } \omega = \omega_0 - \omega_{CM} \end{aligned}$$

In this case, in addition to an internal transition one phonon is created or annihilated.

The following figure shows a sketch of the different possibilities:

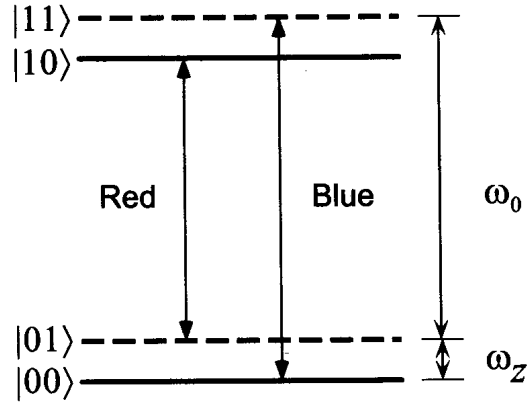


Figure 40: Schematics of possible transitions in a trapped ion [from Nielsen and Chuang]

3.3.3 Single qubit operation

A qubit is encoded in the internal states of the ions:

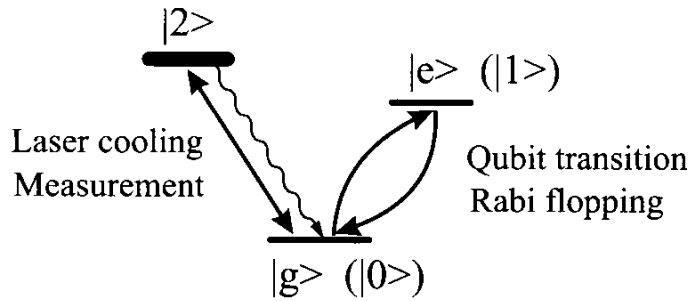


Figure 41: Encoding qubits in a trapped ion [from Bouwmeester et al.]

Single qubit gates are established by tuning the laser to the frequency $\omega = \omega_0$. By choosing the phase shift ϕ and the duration of the interaction appropriately, arbitrary rotations can be performed. Thus, any single qubit-gate can be realized this way.

3.3.4 Two qubit operation

A controlled phase-flip gate can be constructed with the help of an auxiliary atomic level in the following way [J. I. Cirac, P. Zoller, Phys. Rev. Lett. 74, 4091 (1995)]:

1c.

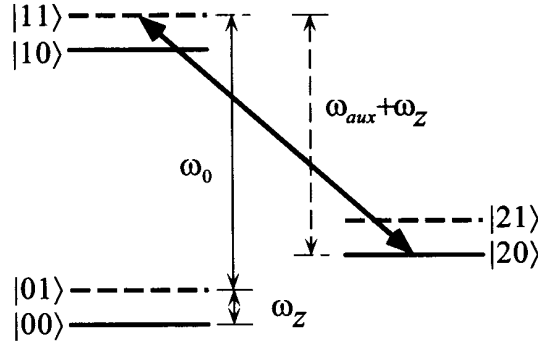


Figure 42: Schematics of a two qubit gate [from Nielsen and Chuang]

1. We first assume that initially one qubit is stored in an ions internal state ($|0\rangle$, or $|1\rangle$), another qubit is stored in the phonon state ($|0\rangle$, or $|1\rangle$). Both qubits can be in any arbitrary superposition.
2. A laser is tuned to the frequency $\omega_{aux} + \omega_z$, to cause the transition between the auxiliary state $|20\rangle$ and only the state $|11\rangle$. Because of the uniqueness of this frequency, no other transitions are excited. The phase and duration of the laser pulse is chosen properly to make a 2π -pulse. This results in

$$|11\rangle \longrightarrow -|11\rangle$$

All other states remain unchanged. Thus the effect on the initial state is:

$$\begin{aligned} (|0\rangle + |1\rangle)_{ion}(|0\rangle + |1\rangle)_{phonon} &= |00\rangle + |10\rangle + |01\rangle + |11\rangle \\ &\longrightarrow |00\rangle + |10\rangle + |01\rangle - |11\rangle \end{aligned}$$

which is the desired controlled phase gate.

3. In order to decode both qubits in ions a SWAP-gate is required which maps an ions qubit state on a phonon qubit state. This can be done by tuning the laser to the frequency $\omega_0 - \omega_z$, and arranging the phase and pulse duration such that a π -pulse is established:

$$(\alpha|0\rangle + \beta|1\rangle)_{ion} \longrightarrow (\alpha|0\rangle + \beta|1\rangle)_{phonon}$$

The interaction between arbitrary qubits is achieved since the phonons are quantized modes of the *center-of-mass* (COM) oscillation shared by all ions in the trap! The COM-mode acts as a *quantum bus* as sketched in the following cartoon:

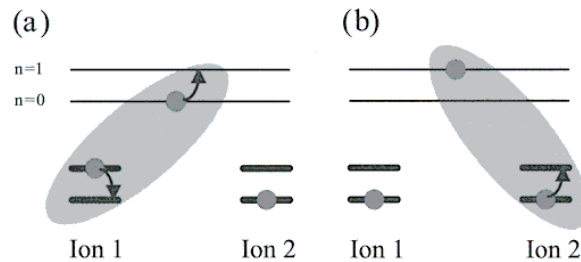


Figure 43: Quantum computation with trapped ions [from Bouwmeester et al.]

A CNOT gate between ion k and ion j can thus be constructed using the following sequence of operations:

$$CNOT_{jk} = H_k \overline{SWAP}_k C_j SWAP_k H_k$$

where C_j is the controlled phase gate on the ion j and H_k are Hadamard gates on ion k .

Any quantum computation can thus be performed with a string of trapped ions!

More recent proposals [J. F. Poyatos, J. I. Cirac, P. Zoller, Phys. Rev. Lett. 81, 1322 (1998)] show that clever techniques exist to perform a quantum computation with somewhat hotter ions, which don't have to be cooled to the Lamb-Dicke regime by Doppler and sideband cooling. For these techniques Doppler cooling alone may be sufficient.

3.4 Experimental Realization of a CNOT Gate

A first demonstration of a CNOT gate was demonstrated in the group of D. Wineland at NIST, Boulder, USA [C. Monroe et al., Phys. Rev. Lett. 75, 4715 (1995)]. (See also <http://www.bldrdoc.gov/timefreq/ion/index.htm>) A single

${}^9\text{Be}^+$ ion was trapped and laser cooled into the motional ground state. The computational basis was:

$$|0\rangle|\uparrow\rangle, |0\rangle|\downarrow\rangle, |1\rangle|\uparrow\rangle, \text{ and } |1\rangle|\downarrow\rangle$$

where $|0\rangle$ and $|1\rangle$ denote the motional states and $|\uparrow\rangle$ and $|\downarrow\rangle$ the internal (hyperfine states). More precisely:

$$\begin{aligned} |\uparrow\rangle &= {}^2S_{1/2} |F=2, m_F=2\rangle \\ |\downarrow\rangle &= {}^2S_{1/2} |F=1, m_F=1\rangle \end{aligned}$$

An additional state was used as auxiliary state,

$$|aux\rangle = {}^2S_{1/2} |F=2, m_F=0\rangle$$

another state was used for detection:

$${}^2P_{3/2} |F=3, m_F=3\rangle$$

The following shows the level scheme and a miniaturized Be-ion trap:

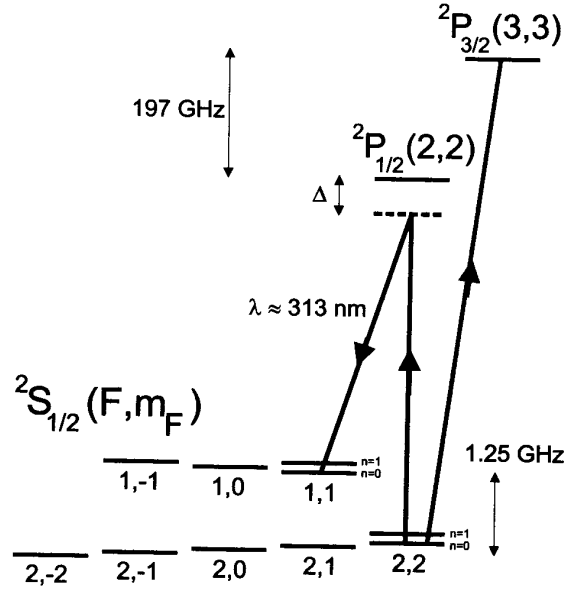


Figure 44: Energy levels of a Be-ion used for experimental demonstration of a CNOT gate [from Bouwmeester et al.]

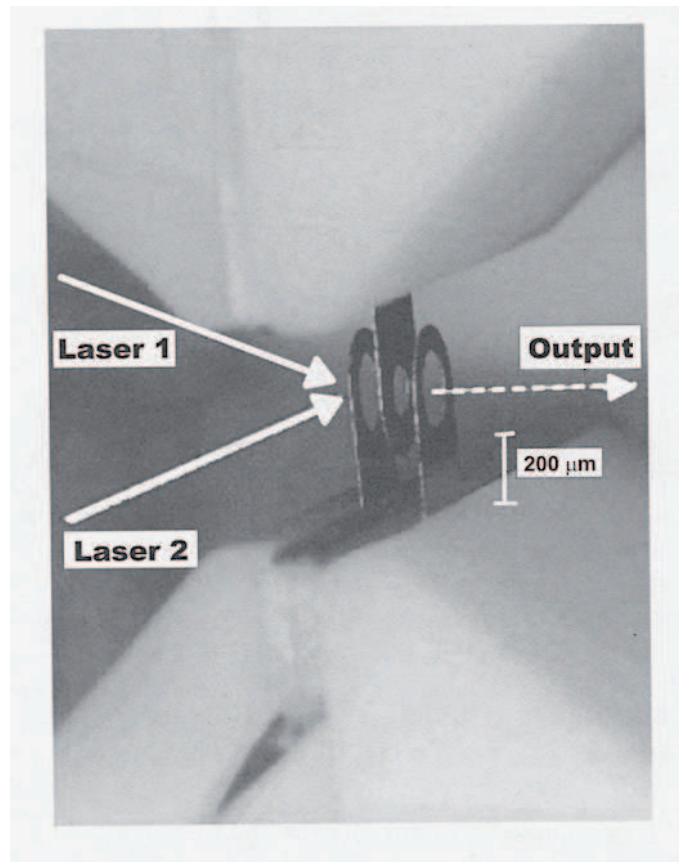


Figure 45: Picture of a miniaturized ion trap [from Nielsen and Chuang]

In order to demonstrate a CNOT gate the following procedure was used:

1. Doppler and sideband cooling of the ion in the $|0\rangle|\downarrow\rangle$ state (95% probability).
2. Initialization in one of the four basis states $|0\rangle|\downarrow\rangle$, $|0\rangle|\uparrow\rangle$, $|1\rangle|\uparrow\rangle$, or $|1\rangle|\downarrow\rangle$ using single qubit rotations.
3. $\pi/2$ -pulse on the internal state. This leaves the motional state unchanged.
4. π -pulse on the $|1\rangle|\uparrow\rangle \rightarrow |aux\rangle$ transition. All other states remain unchanged.
5. $-\pi/2$ -pulse on the internal state. This leaves the motional state unchanged.

6. Detection of the population in the $|0\rangle|\downarrow\rangle$ and $|1\rangle|\downarrow\rangle$ states by shining σ^+ -polarized light resonant to the $^2P_{3/2}$ transition. This measures the internal qubit.
7. Swapping the motional and internal qubit. Then repeat step 6. This measures the motional qubit.

It is easy to verify that the steps 3 to 5 implement a CNOT gate. The following shows the measured CNOT true table:

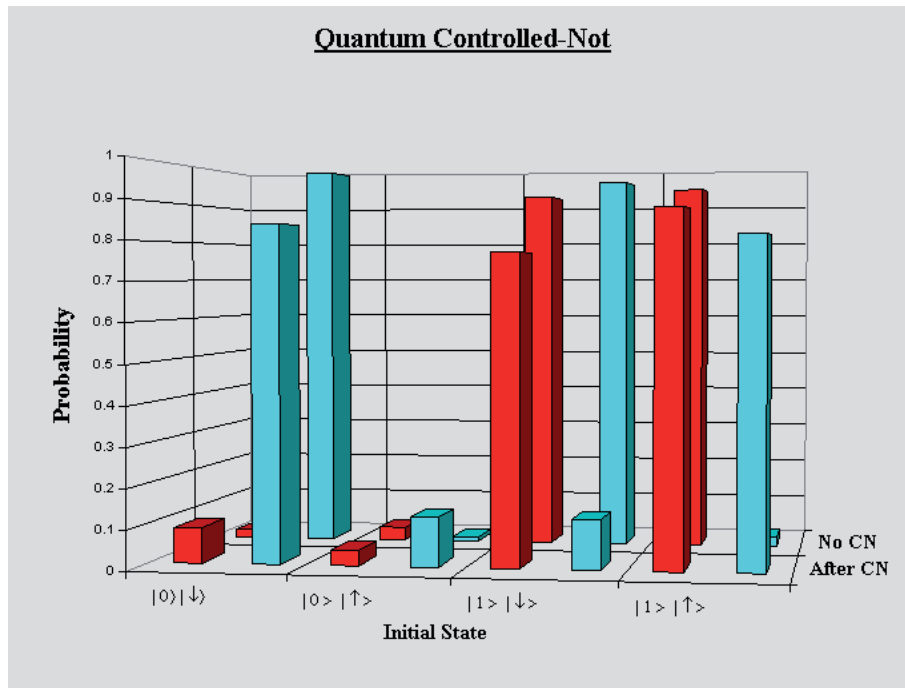


Figure 46: Experimental data of true table for a CNOT gate. [from <http://www.bldrdoc.gov/timefreq/ion/index.htm>]

In order to show that a CNOT gate could be performed on a coherent superposition of qubits with the coherence maintained, the detuning of the $\pi/2$ -pulses was changed. The following shows the resulting so-called Ramsey-fringes for the $|0\rangle|\downarrow\rangle$ and $|1\rangle|\downarrow\rangle$ states.

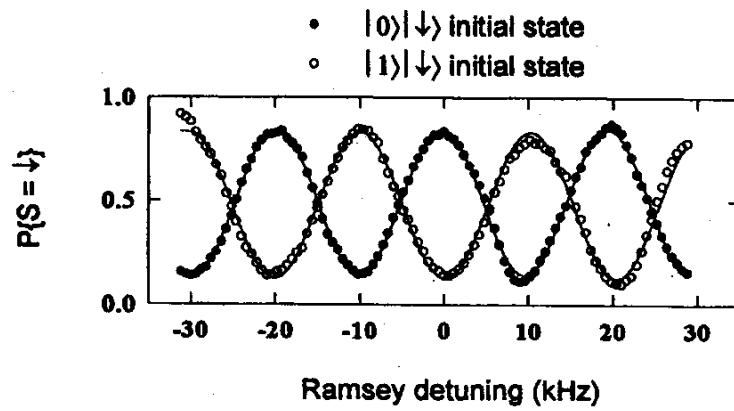


Figure 47: Ramsey spectra of the CNOT gate [from Monroe et al., Phys. Rev. Lett. 75, 4714 (1995)]

The time for the CNOT operations was about 50 microseconds with a measured decoherence time of milliseconds. The main source of decoherence was due to instabilities in the laser intensity, the RF fields and magnetic fields.

3.5 Gates and Tricks with Single Ions

First quantum computing algorithms have been realized, such as the Deutsch-Jozsa algorithm in the Innsbruck group [S. Gulde et al., Nature 421,48 (2003)]. Presently, it is possible to manipulate and individually control up to 10 ions in an ion trap. Quantum teleportation of an unknown quantum state to another was demonstrated by the Innsbruck group [M. Riebe et al., Nature 429, 734 (2004)] and Boulder group [M. D. Barret et al., Nature 429, 737 (2004)]. Also a quantum byte [Häffner et al., Nature 438, 643 (2005)] and a 6-ions GHZ entangled state [D. Leibfried et al., Nature 438, (2005)] were created. In order to obtain even more complex elements novel miniturized ion traps are being developed.

3.5.1 Demonstration of Deutsch-Jozsa

This algorithm was demonstrated by using two qubits. One qubit was implemented in the ground and a metastable state of Ca ions, the $S_{1/2}$ - and $D_{5/2}$ -state respectively. The following picture shows the energy diagramme.

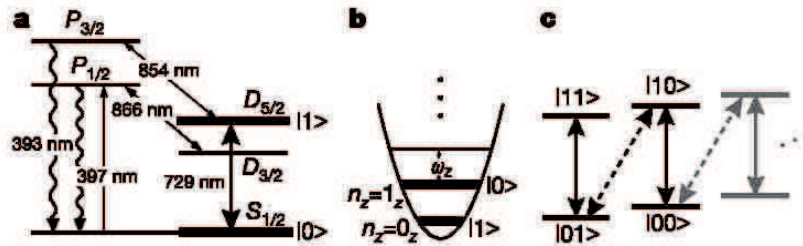


Figure 48: Qubits in the experimental demonstration of the two-qubit Deutsch-Jozsa algorithm [from S. Gulde et al., Nature 421,48 (2003)].

The algorithm (including the function U_f) was encoded by using different laser pulses. Laser frequencies could be tuned with the help of acousto-optic modulators. The following figure shows the probability to find the ion in the upper atomic qubit state. In order to derive this probability the procedure was repeated many times and interrupted after a certain time had elapsed. The experiment shows that it is indeed possible to control a single ion in an ion trap with very high precision. For more complex algorithms the application of the laser pulses will be controlled by a computer. This somewhat approaches techniques which already exist in nuclear magnetic resonance experiments for microwave pulses.

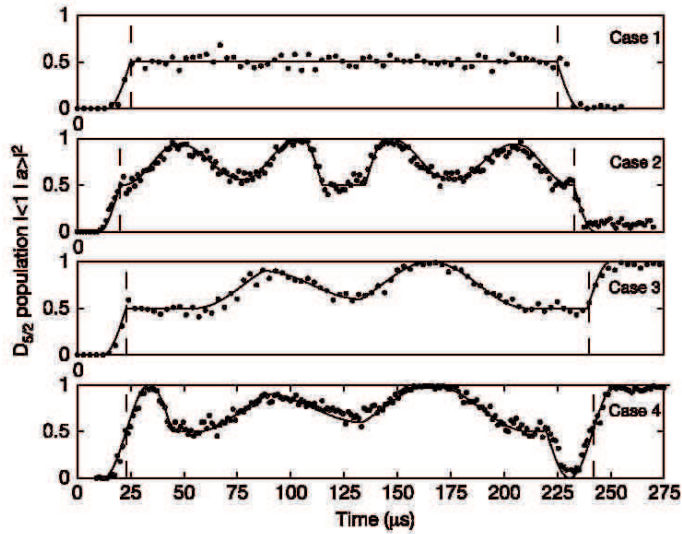


Figure 49: Time evolution of the population of the upper atomic qubit for four different encoded functions [from S. Gulde et al., Nature 421,48 (2003)].

3.5.2 Teleportation of atomic qubits

A recent progress was the demonstration of teleportation of an atomic state from one trapped ion to another. In the Innsbruck group led by Rainer Blatt [M. Riebe et al., Nature 429, 734 (2004)] three ions were manipulated with carefully designed laser pulses. Individual ions could be prevented from disturbance due to detection light by applying so-called "hide"-pulses, which transferred the state to another Zeeman level. The following picture shows the diagram of the algorithm.

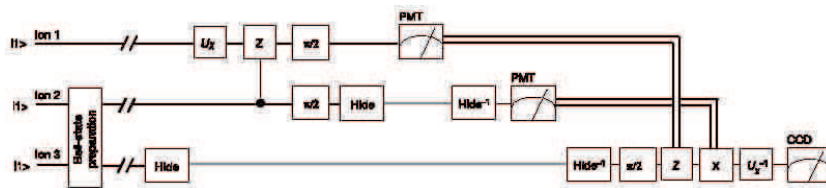


Figure 50: Diagram of the teleportation scheme implemented with three ions [from M. Riebe et al., Nature 429, 734 (2004)].

The implementation of the algorithm consisted of 35 laser pulses including spin echo pulses to revert dephasing. This clearly demonstrates that computer control is essential for an upscaling to more qubits. The following pictures shows

the fidelities for teleportation of different quantum states.

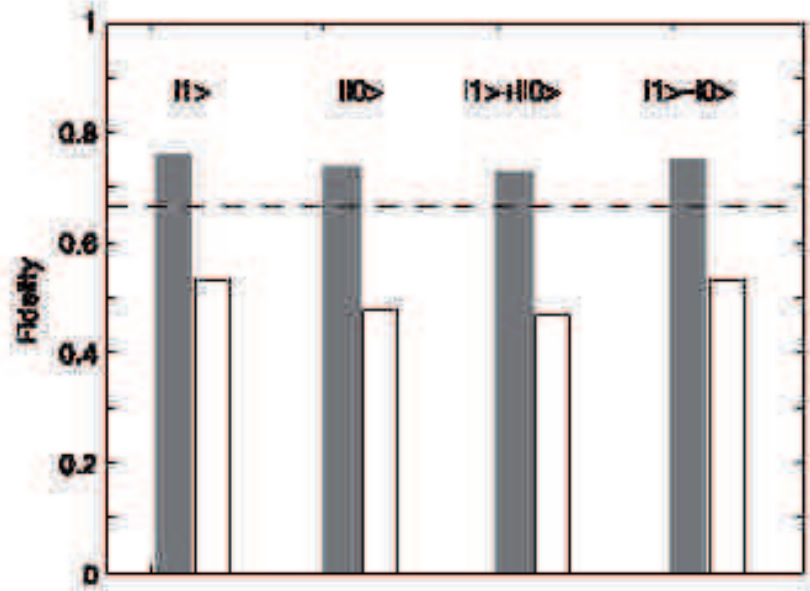


Figure 51: Experimental results for the teleportation of different quantum states [from M. Riebe et al., Nature 429, 734 (2004)].

The group in Boulder led by Dave Wineland followed a slightly different approach. They used a miniaturized ion trap which allowed to move ions from one segment to another. In this way it was also possible to address individual ions with laser pulses. Qubits were encoded in two hyperfine levels of Be ions.

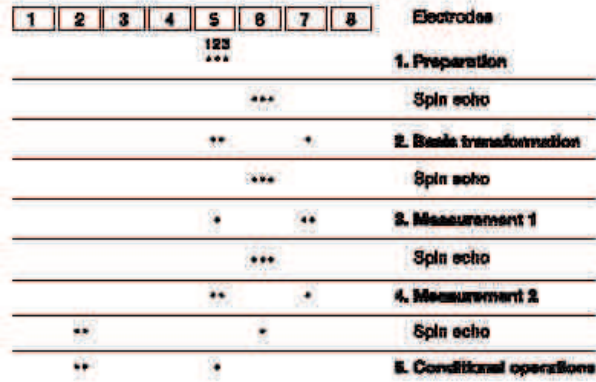


Figure 52: Schematics of the miniaturized ion trap and the position of the different ions during the teleportation sequence [from M. D. Barret et al., Nature 429, 737 (2004)].

In order to demonstrate successful teleportation of arbitrary states a Ramsey interference was measured by applying pulses to ion 1 before and to ion 3 after teleportation.

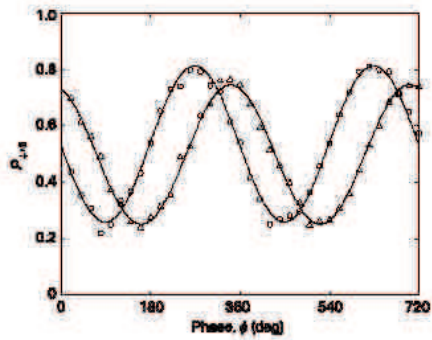


Figure 53: Measured Ramsey interference by applying pulses to ion 1 before and to ion 3 after teleportation for two different phases of the second Ramsey pulse. [from M. D. Barret et al., Nature 429, 737 (2004)]

3.5.3 A Quantum Byte

Linear ion traps allow to trap and cool a large number of atoms. An experimental challenge is to manipulate all trapped ions precisely with tailored laser pulses. Recently, the Innsbruck groups realized a *quantum byte*, i.e., an arbitrary quantum state consisting of 8 quantum bits [Häffner et al., Nature 438, 643 (2005)].

As an example for a complex multi-particle qubit state a *W-state* or *Werner-state* was created. Such a state has a single excitation (one ion in an excited state), but there is no information in which ion.

$$|W_N\rangle = |10000000\rangle + |01000000\rangle + \dots |00000001\rangle$$

In the experiment the 0- and 1-state were realized as the $S_{1/2}$ ground state and the $D_{5/2}$ metastable state in ^{40}Ca -ions. First, all ions were prepared in the state:

$$|W_N\rangle = |0, DDDDDDDD\rangle$$

where the first 0 denotes the motional ground state of center of mass oscillation. Then, ion 1 is flipped by a π -pulse on the carrier transition to

$$|W_N\rangle = |0, SDDDDDDD\rangle$$

Then, most of the population is moved to the $|W_N\rangle = |1, DDDDDDDD\rangle$ state by applying a blue sideband pulse of length $\theta_n = \arccos(1/\sqrt{n})$:

$$\frac{1}{\sqrt{N}}|0, SDDDDDDD\rangle + \frac{\sqrt{N-1}}{\sqrt{N}}|1, DDDDDDDD\rangle$$

This procedure is continued until the final state is reached:

$$|W_N\rangle = \frac{1}{\sqrt{N}}|0, SDDDDDDD\rangle + \frac{1}{\sqrt{N}}|0, DSDDDDDD\rangle + \dots \\ + \frac{1}{\sqrt{N}}|0, DDDDDDDS\rangle$$

The entangled procedure took about 1 *ms*. A major problem is to gain full information of the N-ion complex quantum state. This was obtained via *quantum state reconstruction* by expanding the density matrix in a basis of observables and measuring the corresponding expectation values. In order to do this, a large number (about 650000) additional laser pulses were employed. A full characterization of the state required 10 hours measurement time. A fidelity exceeding 70% were obtained (see reconstructed density matrix in Fig. 54).

The experiment demonstrates that presently there is not only a limit with respect to constructing a complex quantum state, but also to characterize it to full extend, not to mention to perform a tomography of a whole complex quantum gate.

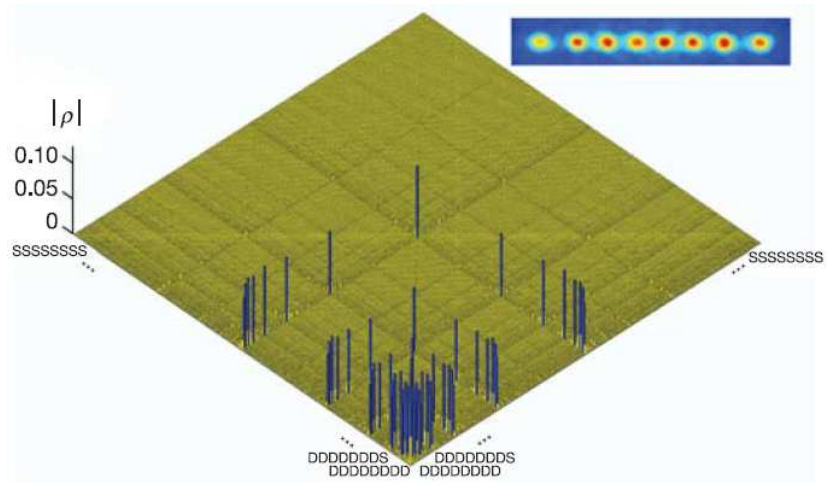


Figure 54: Absolute values, $|\rho|$, of the reconstructed density matrix of a W-state as obtained from quantum state tomography. DDDDDDD...SSSSSSSS label the entries of the density matrix ρ . Ideally, the blue coloured entries all have the same height of 0.125; the yellow colored bars indicate noise. In the upper right corner a string of eight trapped ions is shown. [Häffner et al., Nature 438, 643 (2005)]

3.5.4 Novel Trap Designs

The problem of ion traps as quantum computing devices is their complexity. Ion traps have to be implemented in rather large ultra-high vacuum chambers. The required equipment for lasers and laser control is demanding as well. Figure 55 shows part of the experimental setup (mainly the vacuum chamber), and Fig. 56 a close-up of a linear ion trap.

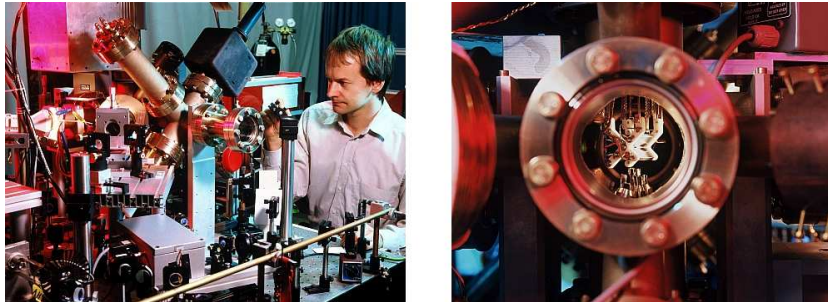


Figure 55: Left: Part of the setup of the ion trap experiment in Innsbruck. Right: Look inside the ultra-high vacuum chamber [from <http://heart-c704.uibk.ac.at/>].

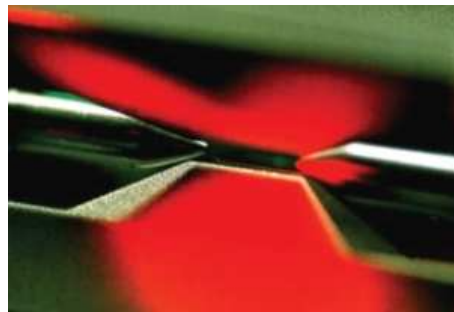


Figure 56: Close-up of a linear ion trap [from <http://heart-c704.uibk.ac.at/>].

A solution to reduce the complexity of ion-trap experiment is to develop miniaturized ion-traps, or *micro-traps* (similar approaches are pursued with traps for neutral atoms as well). Figure 57 shows a standard linear ion trap with four rods together with a layered design suitable for miniaturization. An even simpler design is displayed in Fig. 58.

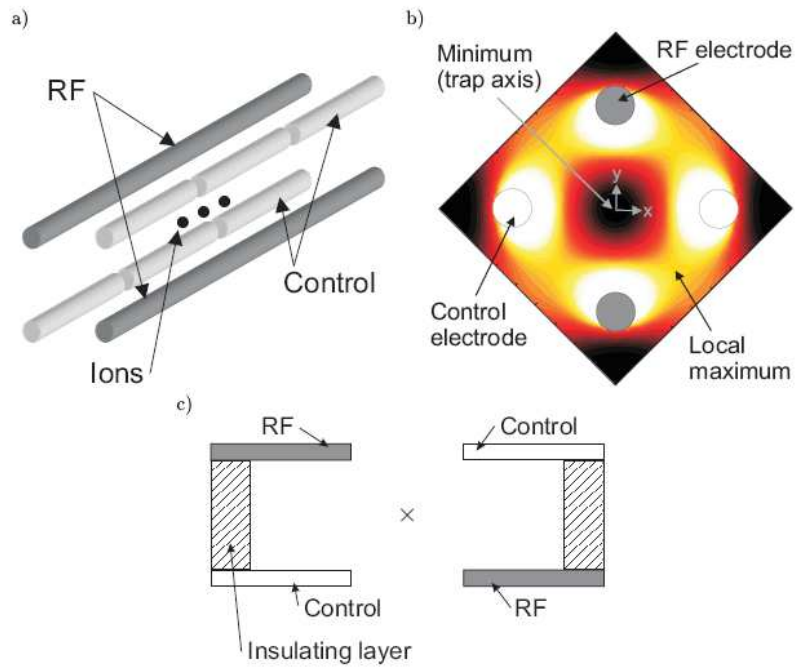


Figure 57: a: Standard four-rod ion trap; b: radial pseudopotential contours; c: Implementation of four-rod design using a layered structure [Chiaverini et al., Quant. Inf. and Comp. 5, 419 (2005)].

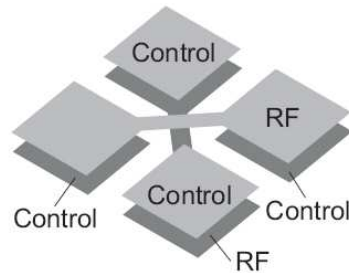


Figure 58: Schematic diagram of a modified two-layer cross to maintain a trapping potential at the center of the cross [Chiaverini et al., Quant. Inf. and Comp. 5, 419 (2005)].

Minaturized surface traps are combined with miniaturized waveguides/antenna for RF radiation required for Paul traps and integrated on chips using standard procedures. Figure 59 shows such a *atom chip*.

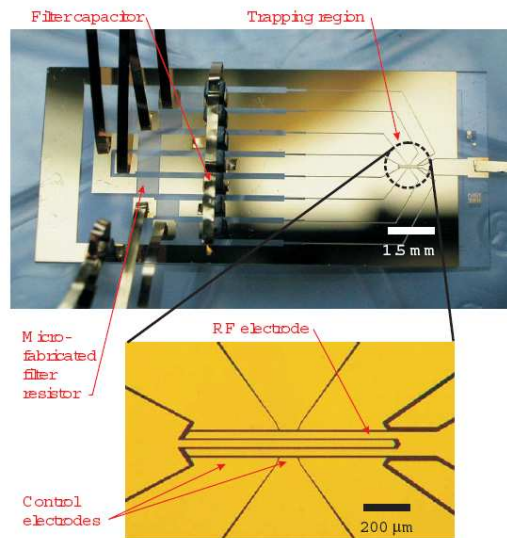


Figure 59: Micrograph of a five wire, one-zone linear trap fabricated of gold on fused silica. The top figure is an overview of the trap chip showing contact pads, onboard passive filter elements, leads, and trapping region. The lower image shows a detail of the trapping region [Chiaverini et al., Quant. Inf. and Comp. 5, 419 (2005)].

It is indeed possible to trap ions on atom chips and to manipulate them in a controlled way (see Fig. 60). A problem is that ions couple strongly to charges and charge fluctuations. Thus, close to surfaces there is an increased heating and decoherence rate which makes it more difficult to maintain coherent operations.

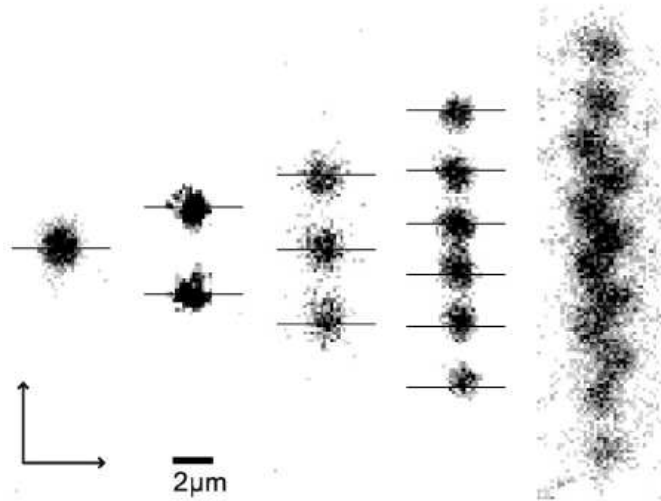


Figure 60: Images of 1, 2, 3, 6, and 12 ions confined in a surface-electrode trap. The length scale is determined from a separate image of the electrodes whose dimensions are known. The horizontal bars indicate the separation distance between the ions as predicted from the measured axial oscillation frequency. The ratio between transverse and axial oscillation frequencies makes it energetically favorable for the 12 ion string to break into a zigzag shape [S. Seidlin et al., PRL 253003 (2006)]

Figure 61 displays another design for a minaturized ion trap. It can be implemented in a standard chip holder to connect all required electrodes (see Fig. 62).

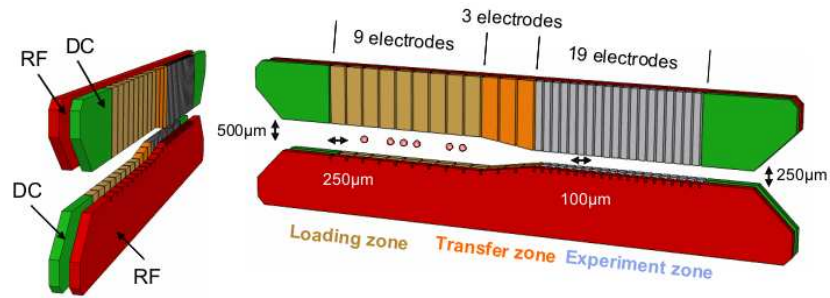


Figure 61: Trap geometry of a minaturized linear ion trap [courtesy F. Schmidt-Kaler].

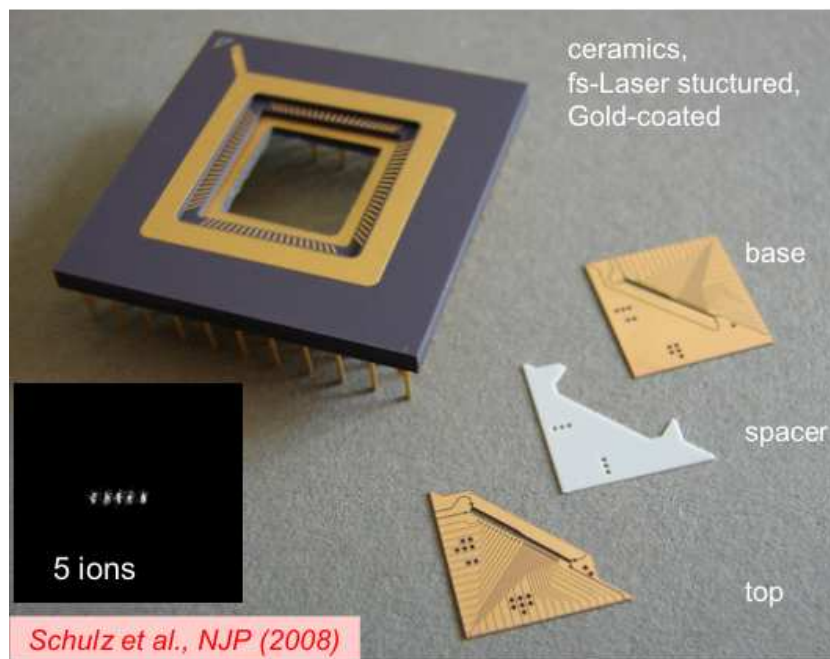


Figure 62: Components for assembling a minaturized ion trap in a chip holder. The inset shows a photo of five trapped ions [courtesy F. Schmidt-Kaler].

There are theoretical proposals how efficient quantum computing can be performed with a large number of ions in minaturized ion traps using only a few ions at a time [Kielpinsky et al., Nature 417, 709 (2002)]. This requires transferring ions to specific locations on an atom chip.

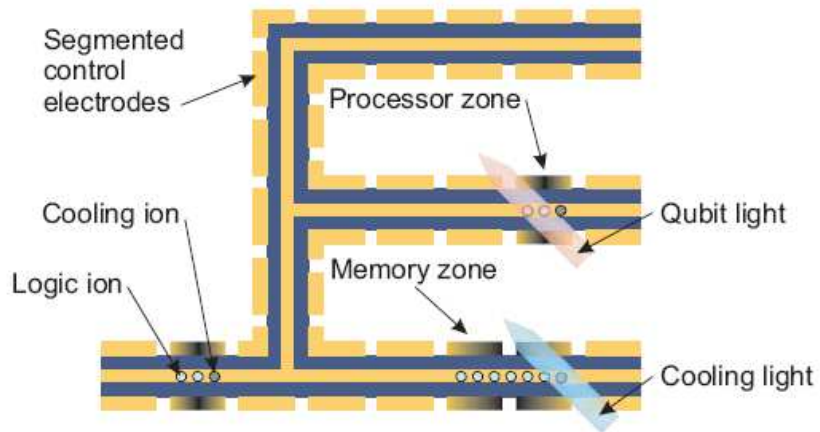


Figure 63: Schematic diagram of a proposed large-scale ion trap array for quantum information processing. Segmented control electrodes allow logic ions (lighter-colored circles) to be transferred to memory and processor regions. After transport ions are recooled by sympathetic cooling (darker-colored circles). [Chiaverini et al., Quant. Inf. and Comp. 5, 419 (2005)]

3.6 Ion trap Cavity QED Systems

One of the problems in the cavity QED-systems introduced in the previous chapters was that the qubits were *flying* qubits (atomic beams were used!). In order to solve this problem there are now attempts to use stored ions in combination with optical cavities.

Two groups in Munich and Innsbruck have successfully stored ions in an ion trap inside high-Q optical cavities.

The Innsbruck group experimentally examines the interaction of a single trapped Calcium ion with a single mode of radiation in a high finesse cavity resonant with the $S_{1/2} - D_{5/2}$ quadrupole transition of the ion. The following pictures show the experimental setup.



Figure 64: Experimental setup of the ion trap cavity-QED experiment in Innsbruck [from <http://heart-c704.uibk.ac.at/>]

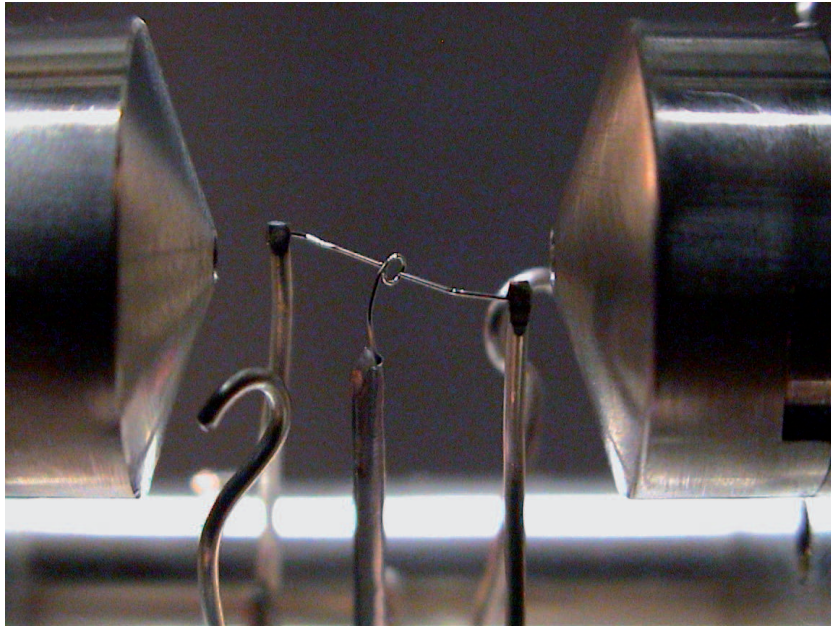


Figure 65: Photo of a Paul trap inside an optical resonator [from <http://heart-c704.uibk.ac.at/>]

The Munich group have successfully demonstrated that they can place a single trapped Calcium ion at will inside an optical resonators [G. Guthörlein et al., Nature, 414, 49 (2001)]. The following pictures show a sketch of the experimental setup and a measurement of fluorescence from the ion. Depending on the position of the ion inside the cavity, the ion is in interaction with a node or an antinode of the standing wave cavity field. Thus, the amount of detected fluorescence light reflects the mode structure of the cavity.

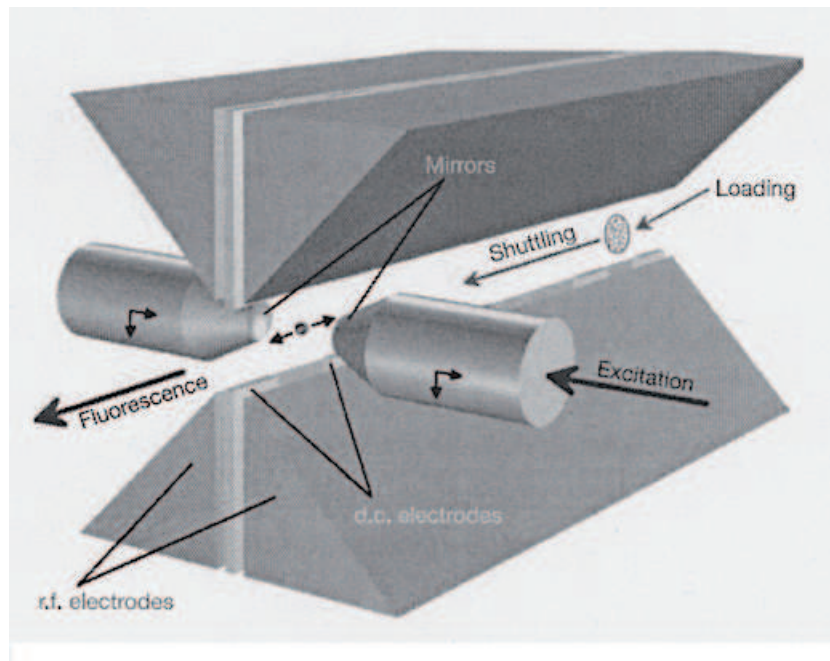


Figure 66: Sketch of the experimental setup in the Munich experiment [from Guthörlein et al., Nature 414, 49 (2001)]

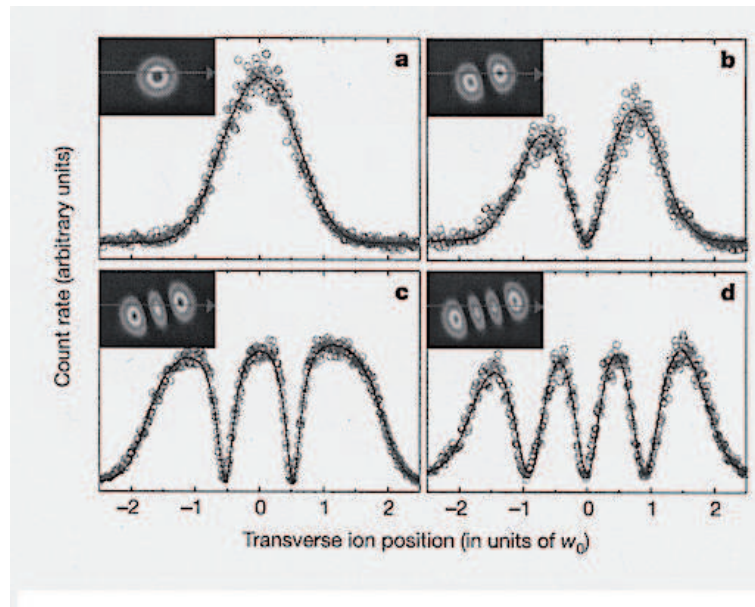


Figure 67: Scattered light from a single trapped Ca-ion in an optical cavity [from Guthörlein et al., Nature 414, 49 (2001)]

It may be very difficult to achieve interaction of many ions with a single or a few modes in such setups. However, these systems may be promising candidates for smaller scale quantum interfaces, where quantum information is stored or manipulated in ions, then transferred to photons, and transmitted to other interfaces. The following shows a sketch of one building block of such a quantum network:

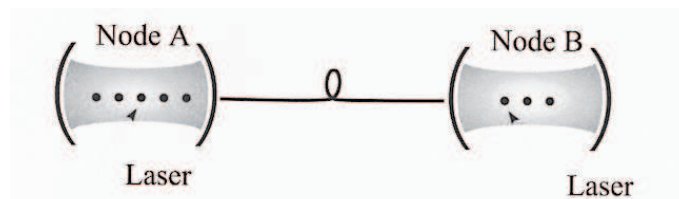


Figure 68: Sketch of a possible quantum network using cavity-QED systems with trapped ions [from Bouwmeester et al.]

3.7 Summary: Ion trap implementation of quantum computers

- **Qubit representation:** Hyperfine ground or metastable states of an atom, and lowest level vibrational modes (phonons) in the trap potential.
- **Unitary evolution:** Arbitrary transforms are constructed from application of laser pulses which externally manipulate the atomic state via the Jaynes-Cummings interaction. Qubits interact via a shared phonon state.
- **Initial state preparation:** Cooling of the atoms into their motional ground state by laser cooling.
- **Readout:** Measure population of the atomic states via fluorescence from an idler state with near unity efficiency.
- **Drawbacks:** Phonon lifetimes are short, ions are difficult to prepare in their motional ground state (many ions tend to form zig-zags or more complicated shapes); some heating mechanisms are unclear. Complexity of laser control increases with number of ions, but atom/ions chips may allow further scaling.

4 Solid State Implementation of Quantum Computers

4.1 Superconducting Qubits

In the following chapter the possible realization of quantum computing devices with conducting nanostructures is outlined. A review of various proposals and techniques can be found in Y. Makhlin et al., Rev. Mod. Phys. 73, 357 (2001), in the special issue of Fortschr. Phys. 48 No. 9-11 (2000), and in Physics Today, Nov. (2005), 42-47.

4.2 Josephson Charge Qubits

4.2.1 Single qubit gates

Charge qubits are represented by different numbers of Cooper-pair charges on a small island. The superconducting state maintains a well defined phase due to energetic separation from the unpaired electrons (Cooper-pair energy gap of the BCS ground state). This gap suppresses decoherence caused by scattering with other electrons. For this reason single (unpaired) electrons can not be used as qubits.

The following figure shows the simplest design of a Josephson charge qubit.

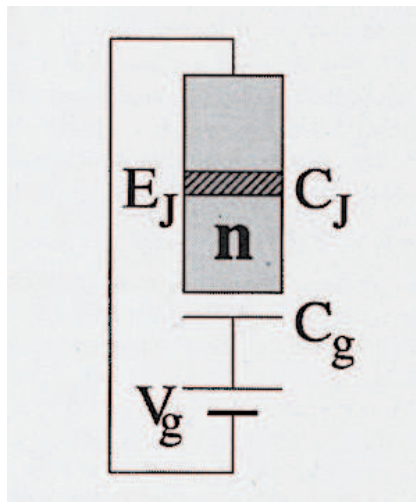


Figure 69: Josephson charge qubit. [from Y. Makhlin et al.]

It consists of a small superconducting island with n excess Cooper-pair

charges (relative to some neutral reference state), connected by a tunnel junction with capacitance C_J and a Josephson energy E_J to a superconducting electrode. A control gate voltage V_g is coupled to the system via a capacitance C_g .

Required temperature:

Capacitances as small as $C_J \leq 10^{-15} F$ can be made. With the single-electron charging energy $E_C = e^2/(C_g + C_J)$ this requires temperature below 1 K.

Reminder Josephson effect:

The Josephson effect occurs when two superconductors are separated by a thin insulator. Tunneling through the insulator is possible, thus the problem is equivalent to a general tunneling problem. The problem can be described by the following Schrödinger equations for the two superconducting states Φ_1 and Φ_2 :

$$\begin{aligned} i\hbar \frac{\partial \Phi_1}{\partial t} &= \frac{qU}{2} \Phi_1 + E_J \Phi_2 \\ i\hbar \frac{\partial \Phi_2}{\partial t} &= -\frac{qU}{2} \Phi_2 + E_J \Phi_1 \end{aligned}$$

where U describes the voltage applied across the junction.

With the ansatz

$$\Phi_i = \sqrt{n_i} \exp(i\phi_i) \quad \text{with electron density } n_i = |\Phi_i|^2$$

one finds:

$$\begin{aligned} \dot{n}_1 &= \frac{E_J}{\hbar} \sqrt{n_1 n_2} \sin(\phi_2 - \phi_1) = -\dot{n}_2 \\ \hbar(\dot{\phi}_2 - \dot{\phi}_1) &= -qU \end{aligned}$$

These equations describe the DC- and AC Josephson effect: Persistent current without an applied voltage, and AC-current with a DC-voltage applied.

If the energy gap is the largest energy in the system, then, at low temperatures, only Cooper-pairs tunnel coherently. The Hamiltonian of the Josephson-qubit is given by:

$$\begin{aligned} H &= 4E_C(\hat{n} - n_g)^2 - E_J \cos \hat{\Theta} \\ &= \sum_n \left\{ 4E_C(n - n_g)^2 |n\rangle \langle n| - \frac{1}{2} E_J (|n\rangle \langle n+1| + |n+1\rangle \langle n|) \right\} \end{aligned}$$

Here, \hat{n} is the number operator (of Cooper-pairs on the island), and Θ describes the phase of the superconducting state on the island. Note that $n_g = C_g V_g / 2e$ is a continuous variable. The energy diagram is plotted in the following figure:

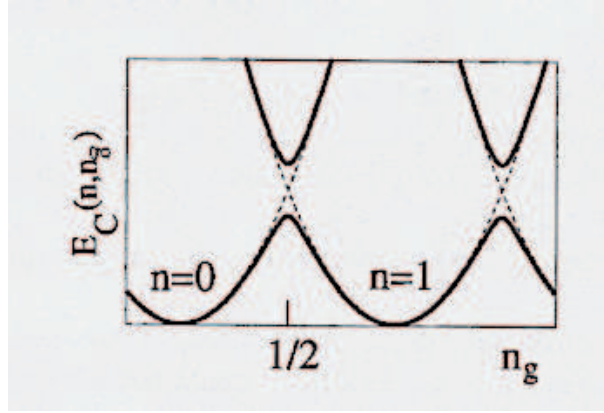


Figure 70: Charging energy of a superconducting electron box. [from Makhlin et al.]

In the vicinity of $n_g = 1/2$ only $n = 0$ and $n = 1$ have to be considered and the Hamiltonian can be written as

$$H = -\frac{1}{2}B_z\sigma_z - \frac{1}{2}B_x\sigma_x$$

with

$$\begin{aligned} B_z &= 4E_C(1 - 2n_g)^2 \\ B_x &= E_J \end{aligned}$$

Obviously arbitrary unitary single qubit rotation can be performed with this Hamiltonian. Since the Josephson energy E_C is relevant only in the vicinity of $n_g = 1/2$ the "field" B_x can be switched on and off by changing the gate voltage V_g and thus n_g .

An improved design, where B_z and B_x can be controlled independently (as required for an ideal single qubit Hamiltonian) is shown in Fig. 71: It consists of a superconducting loop with two Josephson junctions similar as in a SQUID (superconducting quantum interference device). The external flux Φ_x which is controlled via an external magnetic field now determines the Josephson energy E_J :

$$E_J = B_x = 2E_{J0} \cos\left(\pi \frac{\Phi_x}{\Phi_0}\right)$$

where $\Phi_0 = hc/2e$ is the flux quantum.

Now, by changing the gate voltage V_g and the external field (Φ_x), respectively, B_z and B_x can be controlled independently.

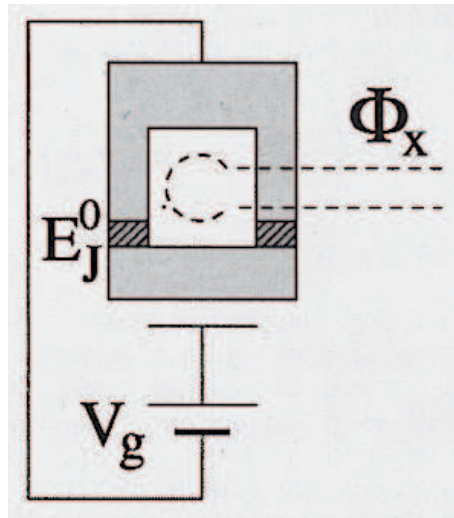


Figure 71: Tunable single Josephson qubit. [from Makhlin et al.]

4.2.2 Experimental Results on Single qubit rotation:

A breakthrough experiment was performed in 1999 by Nakamura (Y. Nakamura et al., Nature 398, 786 (1999)).

The following setup was used:

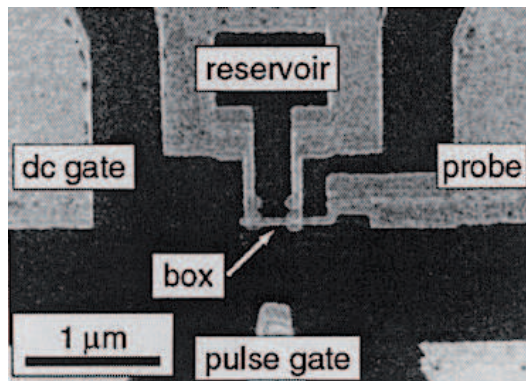


Figure 72:

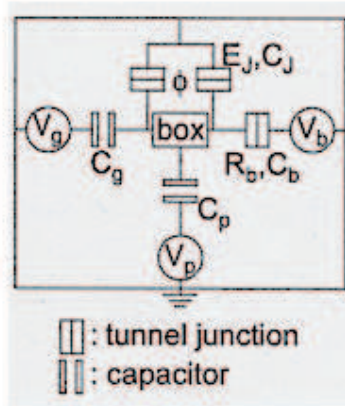


Figure 73: Top: SEM picture of the structure in Nakamura's experiment. Bottom: Circuit diagram of the device. [from Y. Nakamura et al., Nature 398, 786 (1999)]

The experiment realizes a SQUID-type Josephson charge qubit. Two gate electrodes are used to set the bias voltage (V_g and V_p). The voltage V_p is applied in order to quickly switch to a degeneracy point ($n_g \simeq 1/2$). Cooper-pairs on the box leaked out via the probe gate (labeled b) with a time constant of about 6 ns . This was detected as a current via the probe port. The experiment was performed in a dilution refrigerator at 30 mK as follows:

- Initially the box was biased to a point where it was in the zero Cooper-pair eigenstate $|0\rangle$.
- A voltage pulse was switched on for a time Δt to the degeneracy point, where mixing between the two states $|0\rangle$ and $|2\rangle$ occurred.
- Finally, after the voltage pulse the current via the probe port was detected.
- The measurement was performed as a function of the pulse length and the pulse height.

Figures 74 and 75 show the experimental results.

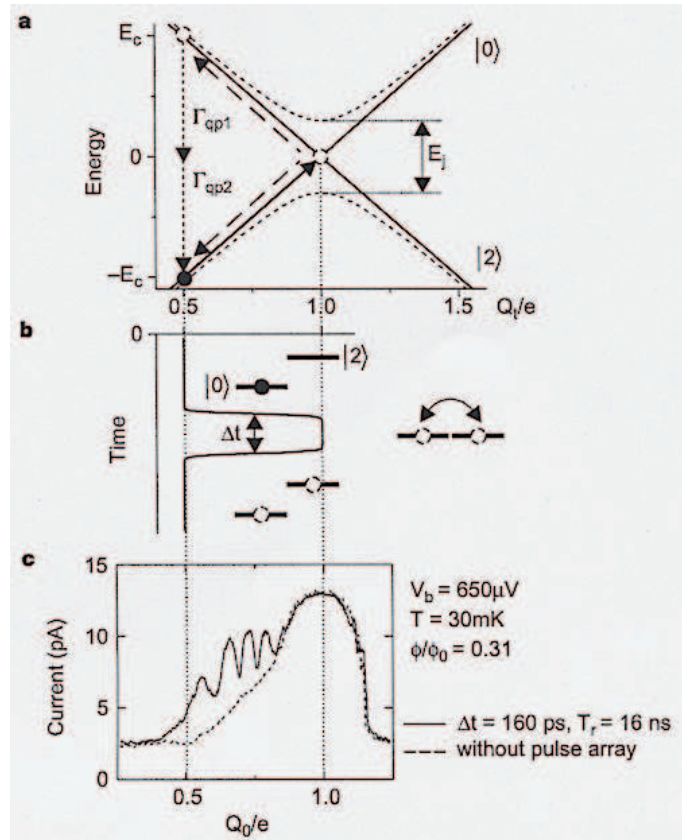


Figure 74: a) Energy diagram illustrating the two charge states as a function of the total gate-induced charge $Q_0 = C_g V_g + C_b V_b$. b) Schematic pulse shape. c) Probe current versus Q_0/e . [from Y. Nakamura et al., Nature 398, 786 (1999)]

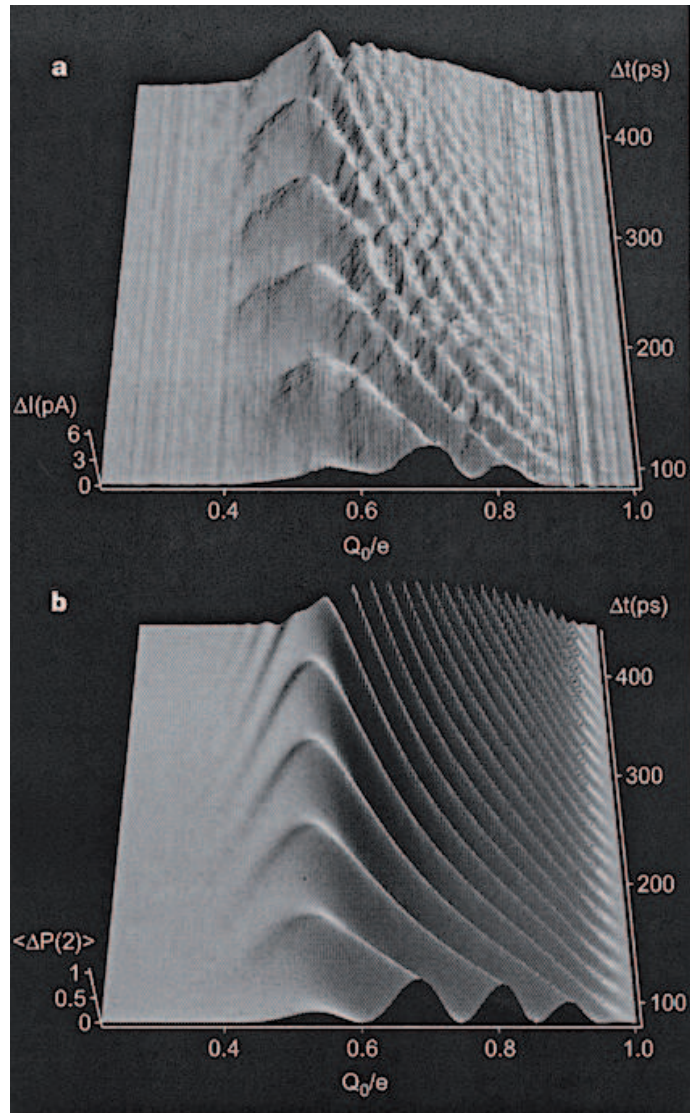


Figure 75: a) Measured pulse-induced current as a function of Δt and Q_0/e . b) numerical simulation [from Y. Nakamura et al., Nature 398, 786 (1999)]

If the difference between the probe current with and without voltage pulse is plotted as a function of pulse duration Δt then a pronounced Rabi oscillation shows up. It has to be mentioned that the decoherence time was determined by the coupling to the probe gate!

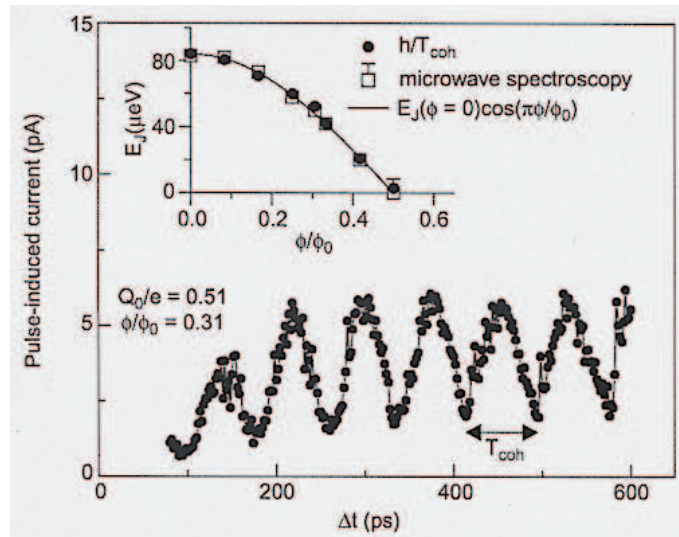


Figure 76: Rabi oscillation in the measured pulse-induced current. The Rabi frequency is determined by the Josephson energy E_J which could thus be measured as well (inset). [from Y. Nakamura et al., Nature 398, 786 (1999)]

4.2.3 Two-qubit gates

In order to perform two-qubit logic gates two qubits have to be coupled. Ideally, the coupling can be controlled. The following shows a schematic of a proposed idea.

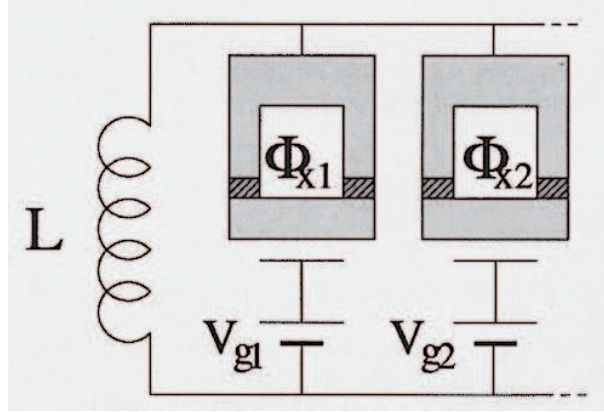


Figure 77: Proposed structure for coupled Josephson qubits. [from Makhlin et al.]

Coupling between two arbitrary qubits is established by oscillator modes in an LC circuit formed by the inductor L and the qubit capacitors. The Hamiltonian for the chain or register of N qubits is:

$$H = \sum_{i=1}^N \left\{ \frac{(2en_i - C_g V_{gi})^2}{2(C_J + C_g)} - E_J(\Phi_{xi}) \cos \Theta_i \right\} + \frac{1}{2NC_{qb}} \left(q - \frac{C_{qb}}{C_J} \sum_i 2en_i \right)^2 + \frac{\Phi^2}{2L}$$

where $C_{qb} = C_J C_g / (C_J + C_g)$, Φ the flux through the common LC-loop, and q the total charge accumulated on the gate capacitors of the array of qubits. In the case that the oscillator modes of the LC-circuit are only virtually excited ($\hbar\omega_{LC} \gg E_J, \delta E_{ch}$) the Hamiltonian can be reduced to (see Makhlin et al.):

$$H = - \sum_{i < j} \frac{E_J(\Phi_{xi}) E_J(\Phi_{xj})}{E_L} \sigma_y^i \sigma_y^j$$

This Hamiltonian is of the desired form for the realization of two-qubit gates. *Note that the two qubit interaction can be switched on and off between arbitrary qubits of the chain!*

Faster qubit operation is achieved if real oscillator quanta of the LC circuits are excited. In this case the LC-circuit acts as a quantum data bus, and the role of the excited oscillator quanta is similar to the phonons in the ion trap quantum computer.

4.3 Josephson Flux Qubits

Charge qubits are defined in a low capacitance regime, where the charging energy dominates over the Josephson energy $E_C \gg E_J$. In the opposite regime $E_C \ll E_J$ the device resembles a SQUID and the flux states are the appropriate eigenstates. The Hamiltonian can be written as

$$H = -E_J \cos\left(\frac{\Phi}{\Phi_0}\right) + \frac{(\Phi - \Phi_x)^2}{2L} + \frac{Q^2}{2C_J}$$

where Φ_x is an external flux, L the self-inductance, and $Q = -i\hbar\partial/\partial t$ the charge. This Hamiltonian again can be written as

$$H = -\frac{1}{2}B_z\sigma_z - \frac{1}{2}B_x\sigma_x$$

with some $B_z(\Phi_x)$ and $B_x(E_J)$.

Qubits are now two clock- and counter-clockwise running persistent currents such that the enclosed flux is an integer multiple of $\Phi_0 = h/2e$. Single qubit rotations can be performed by switching $B_x(E_J)$ on and off. The following shows the schematics of a flux qubit and its equivalent circuit together with an energy diagram.

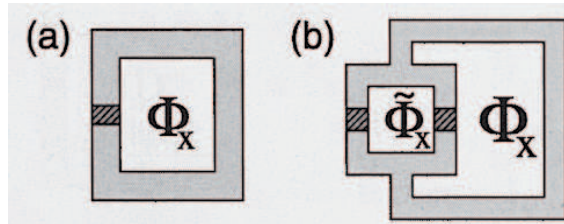


Figure 78: Design of a flux qubit, (a) principle, (b) with controllable Josephson energy [from Makhlin et al.]

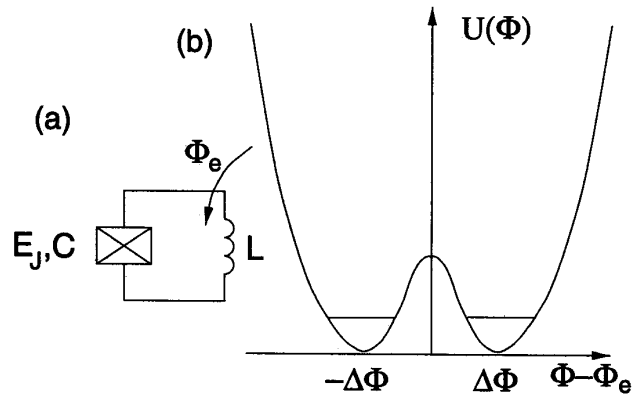


Figure 79: Equivalent circuit (a) and energy diagram (b) of a flux qubit. [from Makhlin et al.]

The energy diagram reveals a double-well potential. Without going into detail the following gives a schematics of two coupled Josephson flux qubits. The dashed line induces a direct inductive coupling, whereas, alternatively, coupling is provided by an external LC circuit. It can be shown

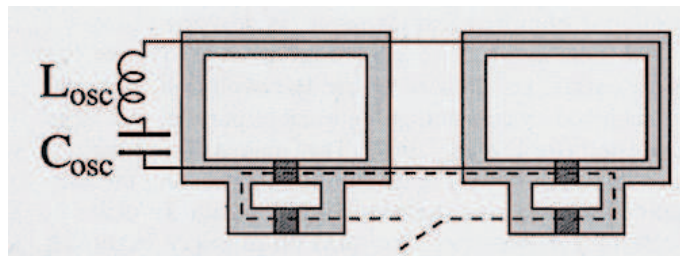


Figure 80: Schematics for two coupled flux qubits [from Makhlin et al.]

that the coupling introduced in this way allows for controlled two-qubit operation, and thus for arbitrary two-qubit gates.

4.4 Readout of Josephson Qubits with SETs

An important issue is the "quiet" read-out of charge or flux qubits. So far a permanent coupling to some probe circuit has been introduced. An Ohmic and thus lossy current in the probe circuit introduces strong decoherence. In order to realize a readout that can be switched on and off it has been proposed to use

a capacitively coupled single-electron transistor: In a single-electron transistor

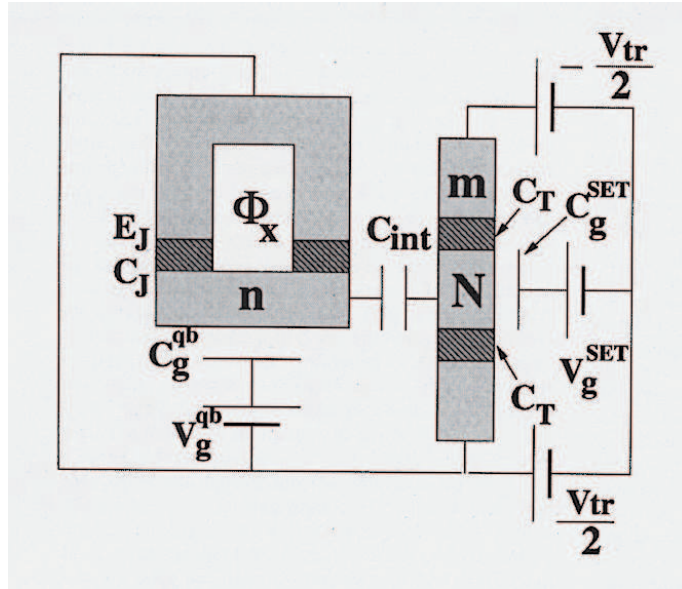


Figure 81: Design for a device where a charge qubit is measured with an SET [from Makhlin et al.]

(SET) the large Coulomb charging energy in a small island N (separated from the leads by insulating barriers with capacitance C_T) allows for electron tunneling only when a certain bias voltages is applied to the gate C_g .

The tunneling current that flows increases with the applied bias voltage and is extremely sensitive to the gate voltage. Detection of a single charge is possible. Furthermore, by changing the gate voltage, the SET can be completely decoupled from the island, and thus decoherence is reduced. Figure 82 and 83 illustrate the operation of an SET.

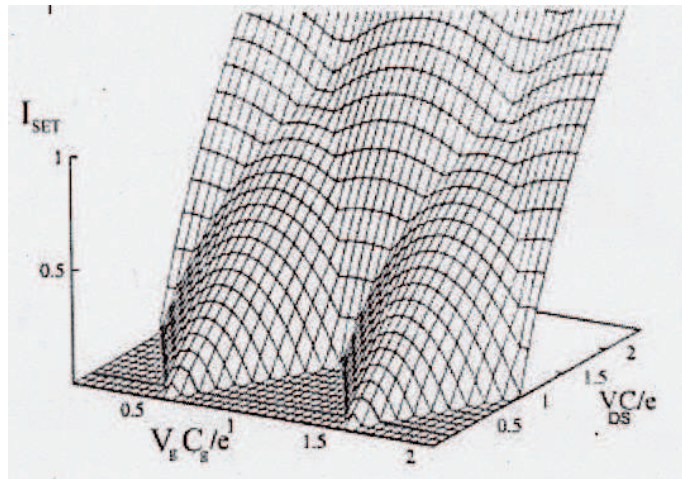


Figure 82: SET current versus gate voltage (V_g) and bias voltage (V_g)

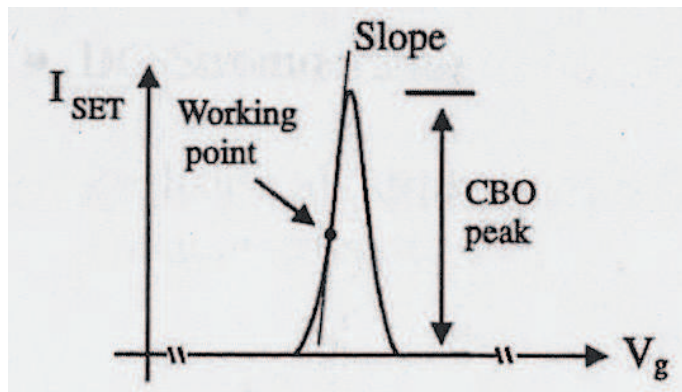


Figure 83: Working point for single charge detection with an SET

Finally, just as an impression of how Josephson quantum computing devices may look like an SET device in a standard microchip holder is shown together with a mount that can be lowered into a dilution refrigerator:

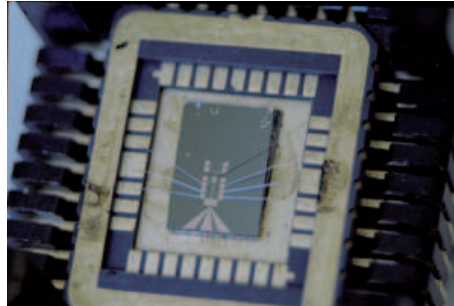


Figure 84: SET device in a standard microchip holder.



Figure 85: Lower part of the cooling finger of a dilution refrigerator.

4.5 Silicon-based Quantum Computation/Spintronics

Large scale *conventional* computation only became possible when thousands of transistors could be integrated onto a single solid state chip. Similarly, it is an attractive idea to implement scalable quantum computers as solid state quantum logical devices. Purest materials and most advanced technology is provided by silicon technology. Since the qubit is usually represented by the spin (nuclear or electron) the implementation of quantum computing devices in the solid state is a part of the new field of *spintronics*. The main focus of spintronics is the realization of devices which do not rely on the charge (electronics!) but on the spin of electrons and holes.

Here we concentrate on a proposal for solid state quantum computation using donor impurities in silicon. Details can be found in *B.E. Kane, Nature, 393, 133 (1998)*.

The proposal by Kane suggests to use single phosphorus (P) atoms implanted as impurities in a silicon crystal (Si). The addition of Column V donors in the Si crystals results in electron states near in the energy to the conduction band, but weakly bound to the donor sites. These states are hydrogen-like, but with an expanded Bohr radius ($a_B \simeq 15 - 30 \text{ \AA}$) and reduced binding energy ($E_b \simeq 10 - 50 \text{ meV}$).

The electron of the ^{31}P -atom has spin 1/2 and silicon (^{28}Si) has spin 0. The nucleus-electron system Si:P with an external magnetic field B along the z -axis is thus:

$$H_{en} = \mu_B B \sigma_z^e - g_n \mu_n B \sigma_z^n + A \sigma^n \cdot \sigma^e$$

where σ are Pauli spin matrices for the electron (index e) and spin (Index n), μ_B and μ_n are the Bohr and nuclear magneton, g_n the nuclear g-factor (for the electrons a g-factor of 2 is approximated), and A is the contact hyperfine interaction energy

$$A = \frac{8}{3} \pi \mu_B g_n |\Psi(0)|^2$$

with the probability density of the electron wave function evaluated at the nucleus $|\Psi(0)|^2$.

The following figure shows the spin energy levels of the P-atom as a function of the magnetic field. The singlet and the triplet states are easily identified.

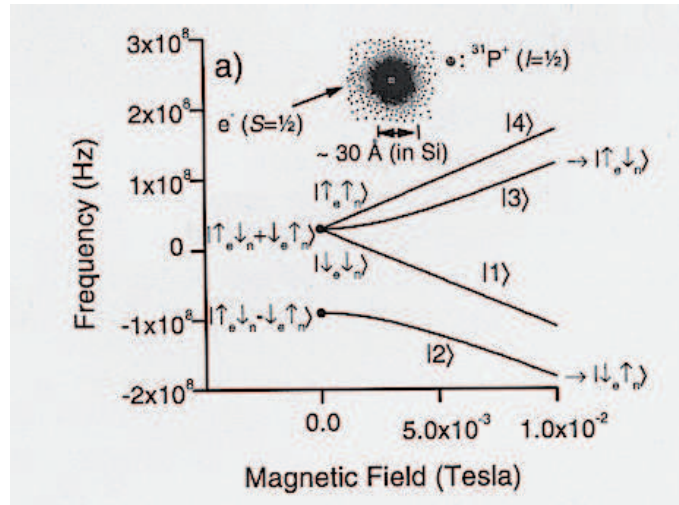


Figure 86: Spin energy levels of ^{31}P in Si. [from Kane, Fortschr. Phys. 48, 1023 (2000)]

Some advantages of the P:Si system are:

- Low spontaneous transition rates between the energy levels:
At temperatures of 1 K the transition time is on the order of 1 hour. Thus, the states can be regarded as meta-stable.
- Narrow linewidth of RF-induced transitions:
In isotopically purified ^{28}Si (silicon has an isotope ^{29}Si with $I = 1/2$) the linewidth is $\leq 1 \text{ MHz}$.
- Low dephasing time T_2 .
 T_2 is on the order of 0.5 msec in isotopically purified Si, probably due to dipolar interactions with other electrons. Decoupling algorithms can be used to further increase T_2 .

4.5.1 Single qubit gates

A qubit is represented by the nuclear spin of the P-atom. Initialization of the qubits is achieved by cooling the sample to very low temperatures in a strong magnetic field. However, active cooling techniques have been suggested, which use controlled coupling to a spin polarized reservoir.

In order to drive single spin rotations a constant RF-field with fixed frequency is applied. Transition are switched on and off resonance with the help of so-called A-gates. The inset of the following picture illustrates the A-gate:

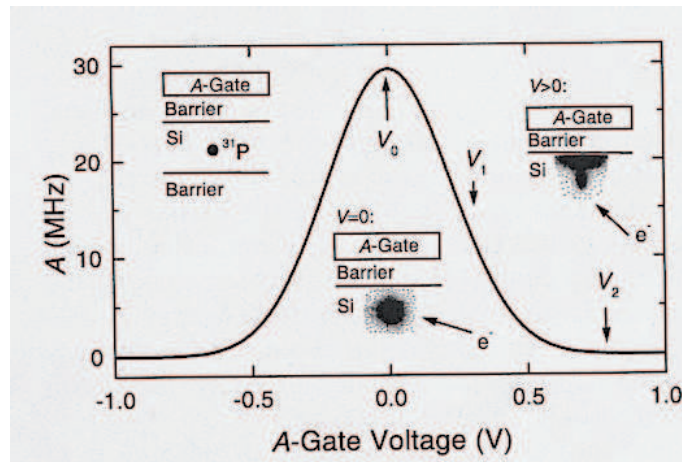


Figure 87: Principle of an A-gate and hyperfine contact energy A versus the applied A-gate voltage. [from Kane, Fortschr. Phys. 48, 1023 (2000)]

The electron wavefunction can be distorted if a positive voltage is applied to the A-gate as shown in the figure. This changes the electron density at the site of the P-atom $|\Psi(0)|^2$ and thus A . Therefore, the resonance frequency for transitions between the spin states can be controlled, and controlled single qubit rotations are possible.

4.5.2 Two-qubit gates

Two qubit gates are realized by a controlled interaction between two qubits, or the two nuclear spins in this case. If two nuclei share a common electron "cloud" then there is an effective interaction between the nuclei mediated by the electrons. This is the so-called J-coupling which is introduced in NMR. Kane proposed to implement so-called J-gates to control the J-coupling between neighboring P-atoms. The following figure shows the schematics:

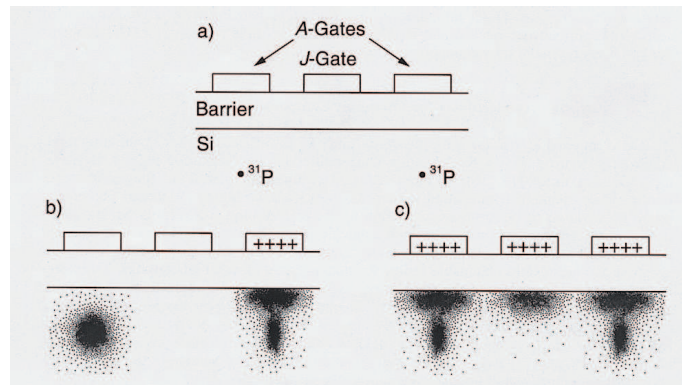


Figure 88: Principle of a J-gate. [from Kane, Fortschr. Phys. 48, 1023 (2000)]

As described above a positive voltage on an A-gate spreads out the electronic wavefunction. If two P donors are very close to each other the electron wavefunction of both atoms can overlap. In order to establish an independent control of single and two qubit interaction, a third J-gate is placed between two A-gates. This J-gate now controls the amount of overlap and thus the amount of J-coupling.

The strength of the J-coupling energy as a function of the distance between neighboring nuclei can be approximated as

$$J(r) \sim E_b \left(\frac{r}{a_B} \right)^{5/2} \exp \left(\frac{-2r}{a_B} \right)$$

This formula can be derived from a model of two well-separated H-atoms. Figure 89 illustrates the behaviour:

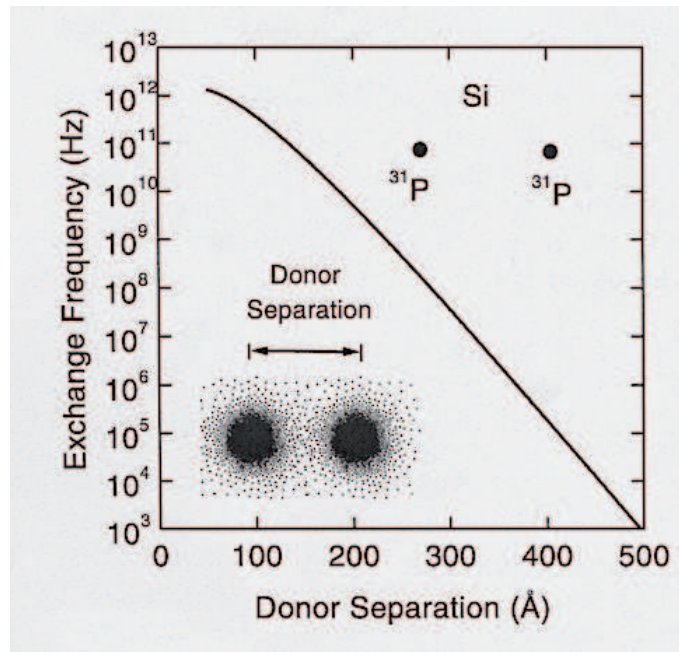


Figure 89: Principle of a J-gate. [Strength of the J-coupling energy between two donor sites as a function of their separation. [from Kane, Fortschr. Phys. 48, 1023 (2000)]

The J-coupling energy can be very large (up to 10^{11} Hz) and can be switched on and off. The controlled two-qubit interaction together with single qubit rotations allows arbitrary quantum computation!

The speed of a silicon quantum computer is limited by single qubit operations which can be performed at a rate of $\approx 10 - 100$ kHz.

4.5.3 Single spin measurement

A very difficult task in the proposed structure is the required read-out of the state of a single spin. A solution could be to transform the problem into the read-out of charge with the help of a single-electron transistor (SET). As discussed in the previous chapter an SET is a very sensitive electrometer capable of detecting single charges.

The proposed strategy is to read-out a two-electron system $|\downarrow?\rangle$, where one electron is in a known spin state. Techniques to prepare electrons in a well defined spin state are known and first experiments have been performed.

A two-electron system can be in one of the following states:

$$\begin{aligned}
 \text{singlet} & : 1/\sqrt{2}(|\downarrow\uparrow\rangle - |\uparrow\downarrow\rangle) \\
 \text{triplet} & : |\uparrow\uparrow\rangle \text{ or} \\
 & \quad |\downarrow\downarrow\rangle \text{ or} \\
 & \quad 1/\sqrt{2}(|\downarrow\uparrow\rangle + |\uparrow\downarrow\rangle)
 \end{aligned}$$

The scattering from the state $1/\sqrt{2}(|\downarrow\uparrow\rangle + |\uparrow\downarrow\rangle)$ to the state $1/\sqrt{2}(|\downarrow\uparrow\rangle - |\uparrow\downarrow\rangle)$ is much faster than the scattering between $|\uparrow\uparrow\rangle$ and $|\downarrow\downarrow\rangle$ since in the latter a spin flip is required. Thus after some time it is sufficient to discriminate a singlet from a triplet state and to detect the unknown spin. Doubly charged donor atoms such as column VI impurities in silicon (e.g. Te) can bind two-electron states. The singlet state is much more strongly bound than the triplet state. This can be used to build a singlet/triplet detector with a column VI donor in silicon and an SET as shown in the following figure:

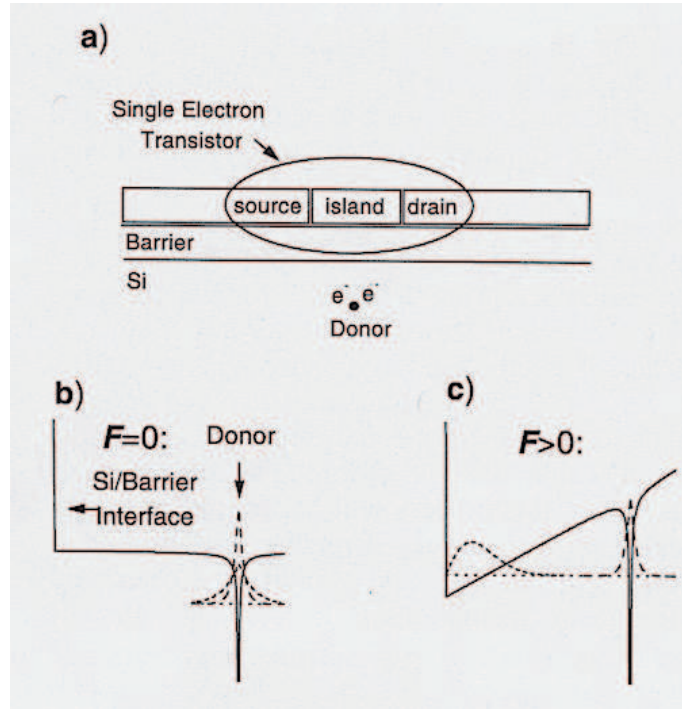


Figure 90: Schematics of a singlet/triplet detector made from a column VI donor in Si. [from Kane, Fortschr. Phys. 48, 1023 (2000)]

If no external electric field is applied then both singlet and triplet states are bound to the donor site. However, if the electric field strength is increased

then first the triplet state is ionized. The ionized electron will be located close to the Si/barrier interface, where it is easily detected by the SET-electrometer. A main drawback of this proposal is that the spin state has to be transferred *coherently* from the qubit donor site to the read-out donor site. This could be established by subsequent swapping between neighboring qubits, but is still a non-trivial task.

Silicon quantum computation is still in its very infancy. However, the individual tasks (control of single donor sites, manipulation of single donors, read-out of single spin) are within the reach of present day technology. Additionally, these tasks are highly important for the fabrication of smaller and smaller conventional computers, which will strongly drive attempts to overcome the problems.

4.6 Quantum Dots as Qubits

In **quantum dots** electrons are confined in all three directions. If the confining structure is small enough the discrete energies of single electron states can be resolved. Due to the analogy with single electrons trapped in the Coulomb potential of a single nucleus, quantum dots are sometimes called *artificial atoms*. The attractive aspect - compared to single atoms - is that the confining potential can be manipulated or even designed at will. There are mainly two different kinds of quantum dots:

- Electrically defined quantum dots
In these dots tiny electrodes confine the electronic motion of a two-dimensional electronic system. The two-dimensional system is either a two-dimensional degenerate electron gas (2DEG) or a thin layer of semiconductor material sandwiched between semiconductors of a higher band-gap (quantum well).
- Three dimensional semiconductor dots
Here, electrons are confined in a nanoscopic amount of semiconductor material surrounded by some matrix material (solution, polymer, glass or a higher-bandgap semiconductor)

The following picture shows the band diagram of an interface of GaAs and $\text{Al}_x\text{Ga}_{1-x}\text{As}$.

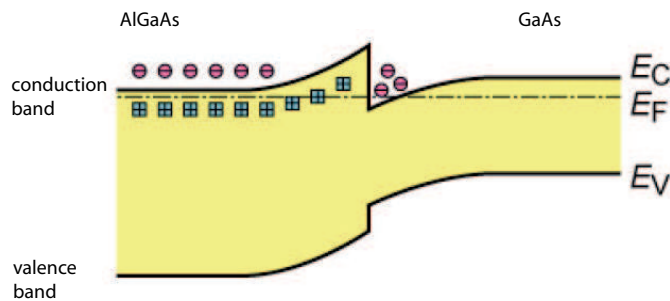


Figure 91: A 2DEG created in a hetero-junction of n-doped AlGaAs and GaAs. The electrons are confined in a triangular shaped potential.

Under certain conditions a thin layer of electrons is formed close to the interface. In this layer the electrons form a quasi two-dimensional system, a

so-called degenerate quantum gas. Additional negatively charged electrodes on top of such a gas confine the electrodes laterally. Figure 92 shows an already rather complex design where 5 quantum dots are defined close to each other.

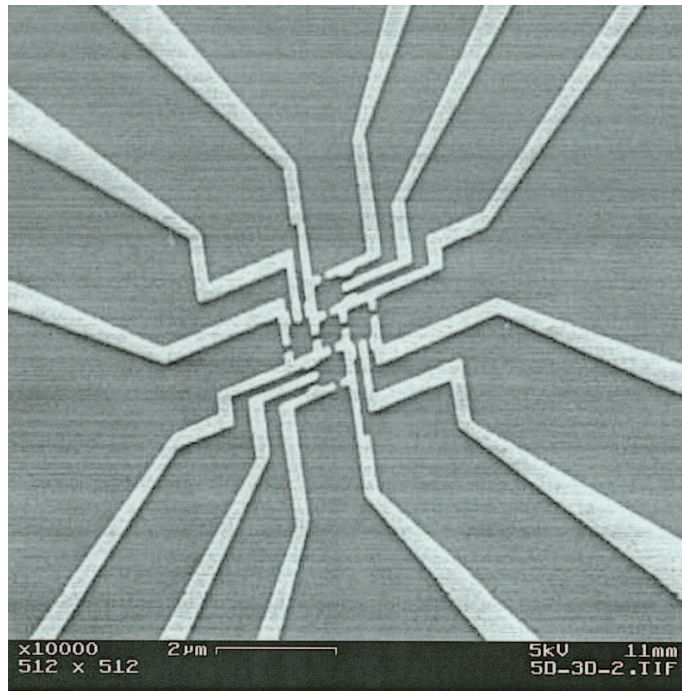


Figure 92: Five coupled quantum dots produced by electric contacts on top of a 2DEG [from <http://www.nano.physik.uni-muenchen.de/Blick/dots.html>]

4.6.1 Fabrication of quantum dots:

Electrically defined quantum dots are made by writing metal electrodes on two-dimensional systems using electron beam lithography, metal evaporation and lift-off techniques.

The following picture shows three possible ways to fabricate three dimensional dots:

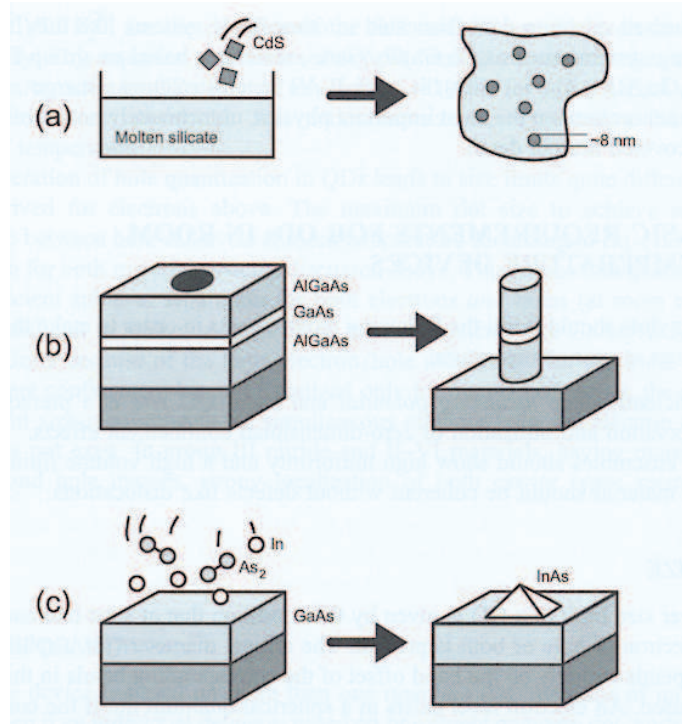


Figure 93: Different approaches to fabricate quantum dots (a) chemical synthesis, (b) artificial patterning of thin film structures, (c) self-organized growth [from D. Bimberg et al., Wiley 1999]

1. Semiconductor quantum dots or (nanocrystallites) can be grown chemically in a glass or various solutions. The typical diameter of these dots is in the order of a few nanometers. The best studied systems so far are II-VI quantum dots (CdSe and CdS).
2. A post can be etched out of a material that contains a quantum well. The disadvantage here is that the confined electrons can interact strongly with surface defects.
3. Under a certain growth condition of a material on a substrate with a different lattice constant (Stranski-Krastanov mode in Molecular Beam epitaxy, MBE, or Metal-organic vapor phase epitaxy, MOVPE) little "droplets"

of semiconductor material form automatically. These quantum dots are sometimes referred to as self-organized quantum dots. Presently, these dots provide the highest quality with respect to optical efficiency and coherence times.

The following picture shows a few InAs quantum dots on a GaAs surface:

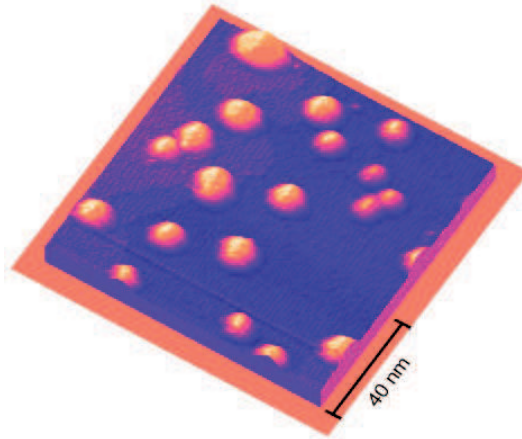


Figure 94: Atomic force microscope picture of single InAs quantum dots on a GaAs surface [from <http://w3.rz-berlin.mpg.de/pc/ElecSpec/>]

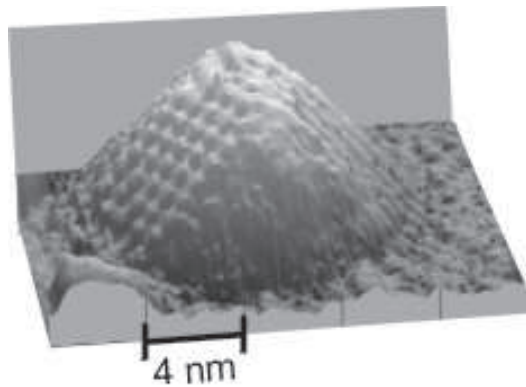


Figure 95: Scanning electron microscope picture of a single InAs quantum dot [from <http://w3.rz-berlin.mpg.de/pc/ElecSpec/>]

4.6.2 Single qubit gates:

The following design shows a proposal by Daniel Loss' group (G. Burkhard et al., Fortschr. Phys. 48, 965 (2000)) for qubits made from coupled quantum dots.

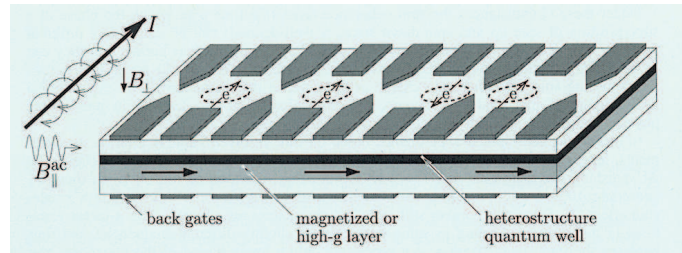


Figure 96: Schematics of an all-electrically controlled quantum dot array [from G. Burkhard et al. Fortschr. Phys. 48, 965 (2000)]

Quantum dots are defined by gate electrodes on top of a quantum well. If a magnetic field is applied perpendicular to the plane of the quantum well a Zeeman splitting between spin-up and spin down-electrons occurs. Transitions between these two qubit levels can be obtained by applying an RF-field. This electron spin resonance (ESR) is in perfect analogy to nuclear magnetic resonance (NMR). Similar as in the case of single donors the ESR resonance frequency can be changed by moving the confined electrons in the direction of a high-g magnetic layer below the quantum well by electrical gating. Thus the electrons can be switched on and off resonance at will. If a constant RF-field with fixed frequency is applied this leads to the realization of arbitrary single qubit rotation.

Another way of coupling dots is used with self-organized dots. The self-organization is driven by the lattice mismatch of the substrate and quantum dot material, respectively. If an additional layer of quantum dots is grown on top of a first layer, then the localized strain caused by the buried quantum dots in the first layer acts as a "seed" for self-organized growth in the second layer. Then, quantum dots predominantly grow as stacks on top of each other.

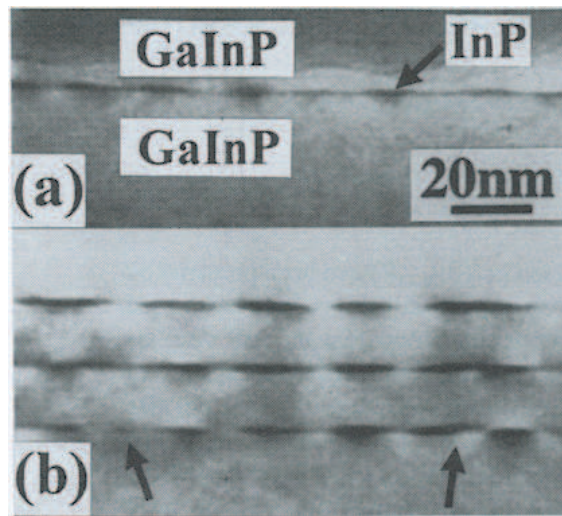


Figure 97: Transmission electron microscopy (TEM) pictures of a single (a) and three (b) layers of quantum dots. The dots tend to be stacked on top of each other. [from Zundel et al. Appl. Phys. Lett. 71, 2972 (1997)]

The coupling (J-energy) between stacked dots of different size can be switched on and off by applying an in-plane electric field as illustrated in the following figure

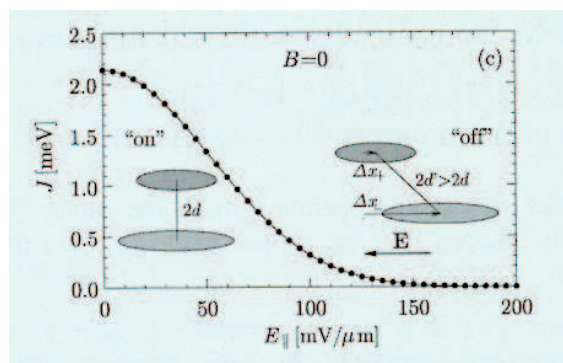


Figure 98: Controlling the coupling (J-energy) of two stacked dots of different size with an in-plane electric field. [from Zundel et al. Appl. Phys. Lett. 71, 2972 (1997)]

4.6.3 Two-qubit gates:

As already illustrated in the previous subsection two qubit gates are implemented by lowering the potential barrier between adjacent dots. Then tunneling occurs similar as in the Josephson charge qubit. An effective two dot molecule is formed. After a well defined time the tunneling barrier can be raised again. Without giving details it is obvious that this procedure allows arbitrary two-qubit operation. In summary, arbitrary quantum gates can be realized this way. The limit of switching speed is given by single qubit rotations, which can be performed within a few 10 psec.

4.6.4 Initialization and read-out

Initialization of n qubits can be realized thermally if the relation

$$g\mu_B B \gg kT$$

is fulfilled. In contrast to nuclear magnetic resonance where only B (liquid phase) or B and T (solid phase) can be changed, here manipulation of g is possible as well.

More advanced methods have been proposed where spin polarization is achieved by coupling of the qubits to a spin polarized reservoir.

Similar as in the case of silicon quantum computing the problem of single spin detection could be circumvented by translating the spin into a charge information. Additionally, possible elements like spin selective barriers have been discussed which would be similar to polarizers in optical devices.

4.6.5 Optical manipulation of quantum dots

Semiconductor quantum dots offer the possibility of optical manipulation. The following picture shows the fluorescence intensity of a sample of single quantum dots. At low density (single quantum dot level) sharp lines could be identified, which correspond to optical transitions between the discrete energy levels of electrons and holes in the quantum dots. The observation of this discrete spectrum also motivated the notation "artificial atoms".

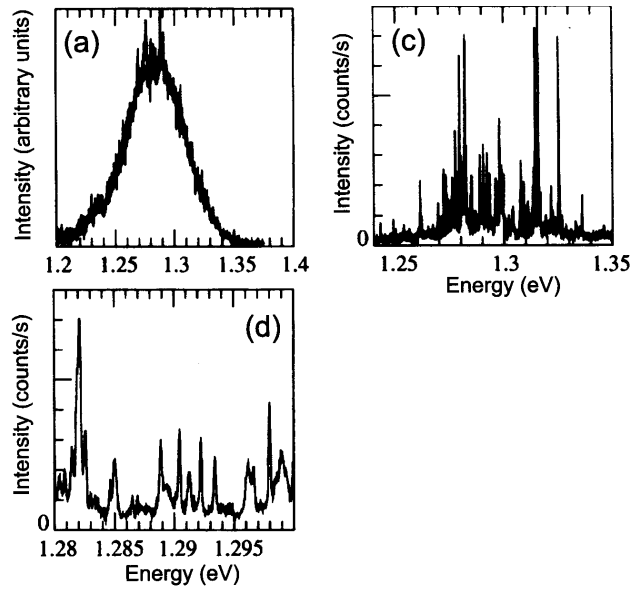


Figure 99: Photoluminescence (PL) spectrum of InAs quantum dots on a GaAs substrate. (a) shows an ensemble of many dots whereas in (b) discrete lines from single dots are resolved. (c) is the same as (b), but with a lower excitation intensity. [from D. Bimberg et al. Wiley 1999]

With the help of narrow-band laser it is thus possible to excited a single electron hole pair. A qubit in this system could also be represented by

$$\begin{aligned} |0\rangle &= |0\rangle_{electron} |0\rangle_{hole} \\ |1\rangle &= |1\rangle_{electron} |1\rangle_{hole} \end{aligned}$$

Single qubit rotations are realized by applying optical pulses of a certain pulse area. One obstacle of using optical excitations as qubits is the relatively short coherence time which is given by the spontaneous decay time of about 1 ns

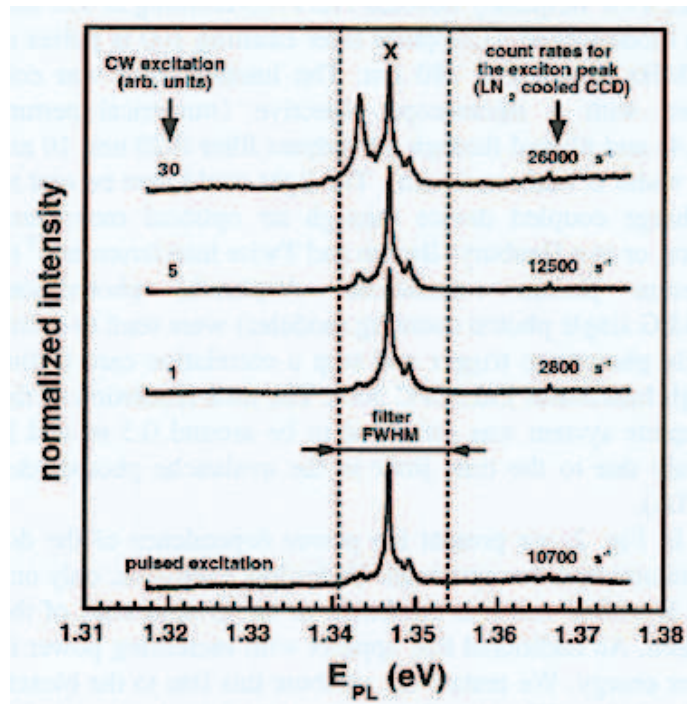


Figure 100: Photoluminescence of a single quantum dot as a function of the excitation power [from V. Zwiller et al., Appl. Phys. Lett. 78, 2476 (2001)]

which has to be compared to the spin decoherence time (e.g. of a single electron in a quantum dot) which is believed to exceed 100 ns.

Nevertheless, since the polarization of the light and the spin state of the electron-hole pair are correlated, optical manipulation is attractive for the following reasons:

- The spin state of the electron can be controlled by the polarization of the laser light which is used for excitation.
- An optical single spin measurement is possible by measuring the polarization of the fluorescence light or by detecting the Farady rotation of an optical probe pulse.
- Quantum information, which can be more easily manipulated in an electronic system, may be transferred into an optical system (photons). Photons are ideal transmitters of quantum information. Possible realization of such quantum electro-optical interfaces are the topic of present research.

- Cavity quantum electrodynamics (QED) can be combined with quantum information processing in solid state systems.

Finally, the following illustrates a proposal (A. Imamoglu et al., Phys. Rev. Lett. 83, 4204 (1999)) where optical manipulation of the spin of single electrons in quantum dots with the help of cavity-QED effects is suggested. The proposed structure consists of a microdisc resonator which contains several quantum dots (see schematics below). These structures have been realized successfully (see figure below).

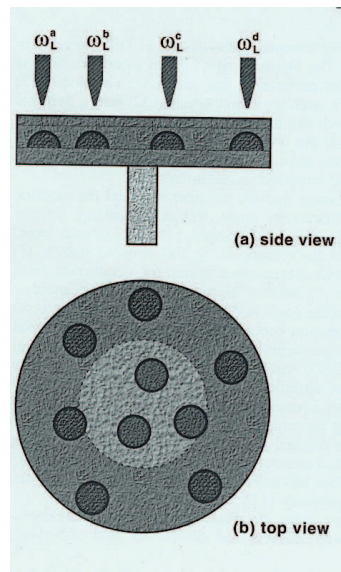


Figure 101: Schematics of a microdisk resonator containing a few quantum dots. It is supposed that each dot can be optically excited with the help of optical fibers. [from A. Imamoglu, Fortschr. Phys. 48, 987 (2000)]

The proposal relies on the possibility to excite optical Raman transitions which induce a spin flip of a single electron in a quantum dot. The dots are embedded in a microdisk and can be excited individually with the help of optical fibers. Qubits are represented by the electron spin eigenstates along the x -axis which is defined as the quantization axis by a magnetic field B_x . Single qubit gates are Raman rotations when the two-photon resonance condition is fulfilled for a single quantum dot. Two qubit gates are established if the Raman resonance condition is fulfilled between two quantum dots which share a common mode of the microdisk resonator.

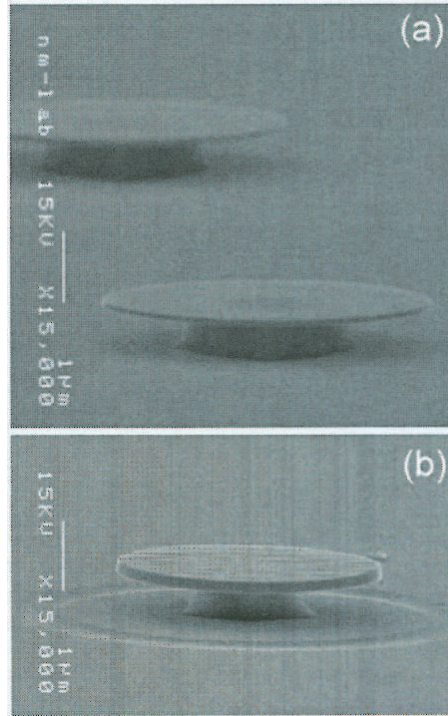


Figure 102: Scanning electron microscope (SEM) image of microdisk resonators.

Since the optically excited states are excited only virtually, decoherence is much reduced in this system. An effective spin-spin interaction between two quantum dots can be realized. The following shows a schematics of the transitions which are involved, where ω_L and ω_{cav} denote the two laser and cavity fields, respectively.

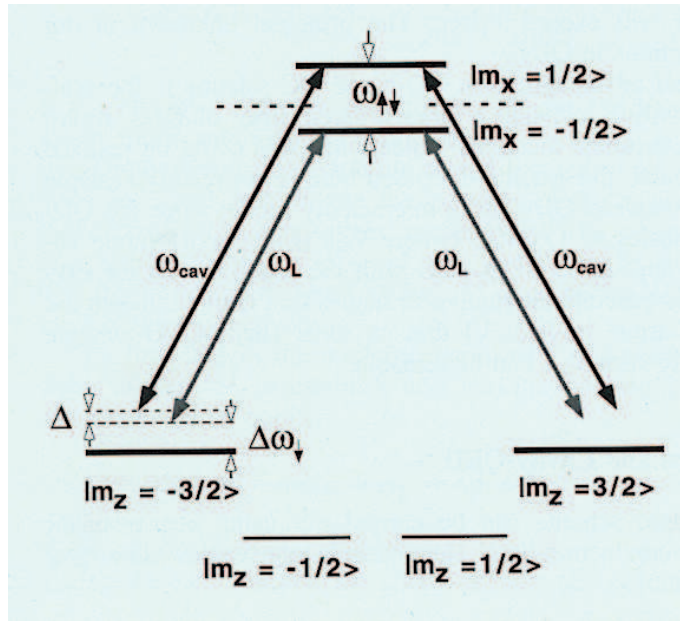


Figure 103: Relevant energy levels for Raman spin flip transition in a quantum dot [from A. Imamoglu, Fortschr. Phys. 48, 987 (2000)]

More recent approaches utilize so-called photonic crystal membrane structures with embedded quantum dots [A. Badolato et al., Science 20, 1158 (2005)]. Photonic crystals are dielectrics with a periodic modulation of the index of refraction. Energy bands occur where light with a frequency within the band cannot propagate anymore. A realization of a photonic crystal is a free standing membrane with periodic holes. Missing holes introduce defects of the periodicity. Close to these defects light can be tightly confined as in a resonator. As shown in Fig. 104 it is possible to couple only a single quantum dot to such a resonator. This is the solid-state analogy of a single trapped atom in an optical cavity.

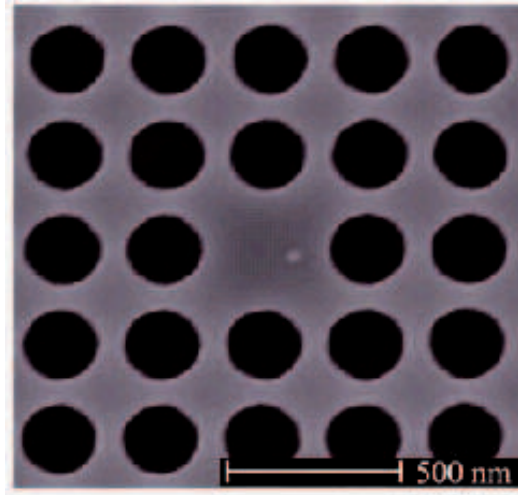


Figure 104: SEM picture of a photonic crystal membrane with single quantum dot in a defect [A. Badolato et al., Science 20, 1158 (2005)].

4.7 Summary: Solid State Implementation

- **Qubit representation:** (a) *Josephson qubits:* Charge or flux. (b) *Silicon QC and quantum dots:* Electron spin.
- **Unitary evolution:** (a) *Josephson qubits:* Arbitrary single qubit operation is obtained by switching on the B_x and B_z part of the single-qubit Hamiltonian. This is achieved by changing a gate voltage or controlling an external magnetic flux. Controllable two-qubit operation between arbitrary two qubits is established by coupling qubits with a common LC circuit. (b) *Silicon QC and quantum dots:* Single qubit rotations are induced by RF-spin resonance pulses. Usually, the RF-frequency is kept constant and the resonance frequency is switched. Two-qubit gates are implemented by coupling the two spins. In order to achieve this either a barrier between the separated qubits is lowered or the electronic wave functions are spread out and overlap for a certain time.
- **Initial state preparation:** (a) *Josephson qubits:* Initial state preparation at low temperature can be realized by setting appropriate gate voltages or applying short gate voltage pulses. (b) *Silicon QC and quantum dots:* Cooling in a strong magnetic field or active spin polarization by coupling the qubits to a spin polarized reservoir.
- **Readout:** (a) *Josephson qubits:* Measurement of a current through a

probe gate or determining the charge with the help of a single-electron transistor. (b) *Silicon QC and quantum dots*: Detection of singlet/triplet state and charge detection with a single-electron transistor. Spin selective barriers.

- **Drawbacks:** (a) *Josephson qubits*: Low temperature operation (dilution refrigerators) is required to reduce the thermal energy below single-electron charging energy or "single-flux" Josephson energy. Charged particles are very sensitive to background charges. The flux is sensitive to stray magnetic fields. (b) *Silicon QC and quantum dots*: Low temperature operation. Fast decoherence rates require very fast switching. Single spin detection is very difficult.